The Earth's Ionosphere: Achieved results in the frame of the CSES-Limadou Scienza +

Giulia D'Angelo on behalf of CSES-Limadou Collaborations

Why the Ionosphere??

CSES-01 orbits sun-synchronously at an altitude of ~500 km

(<u>Top side ionosphere</u>)

- with an inclination of 97.4°
- with descending and ascending nodes at ~14:00 local time (LT) and ~02:00 LT, respectively, and a revisit period of 5 days;
- with an average speed of ~7.2 km/s;
- with an orbital period of ~94 minutes.

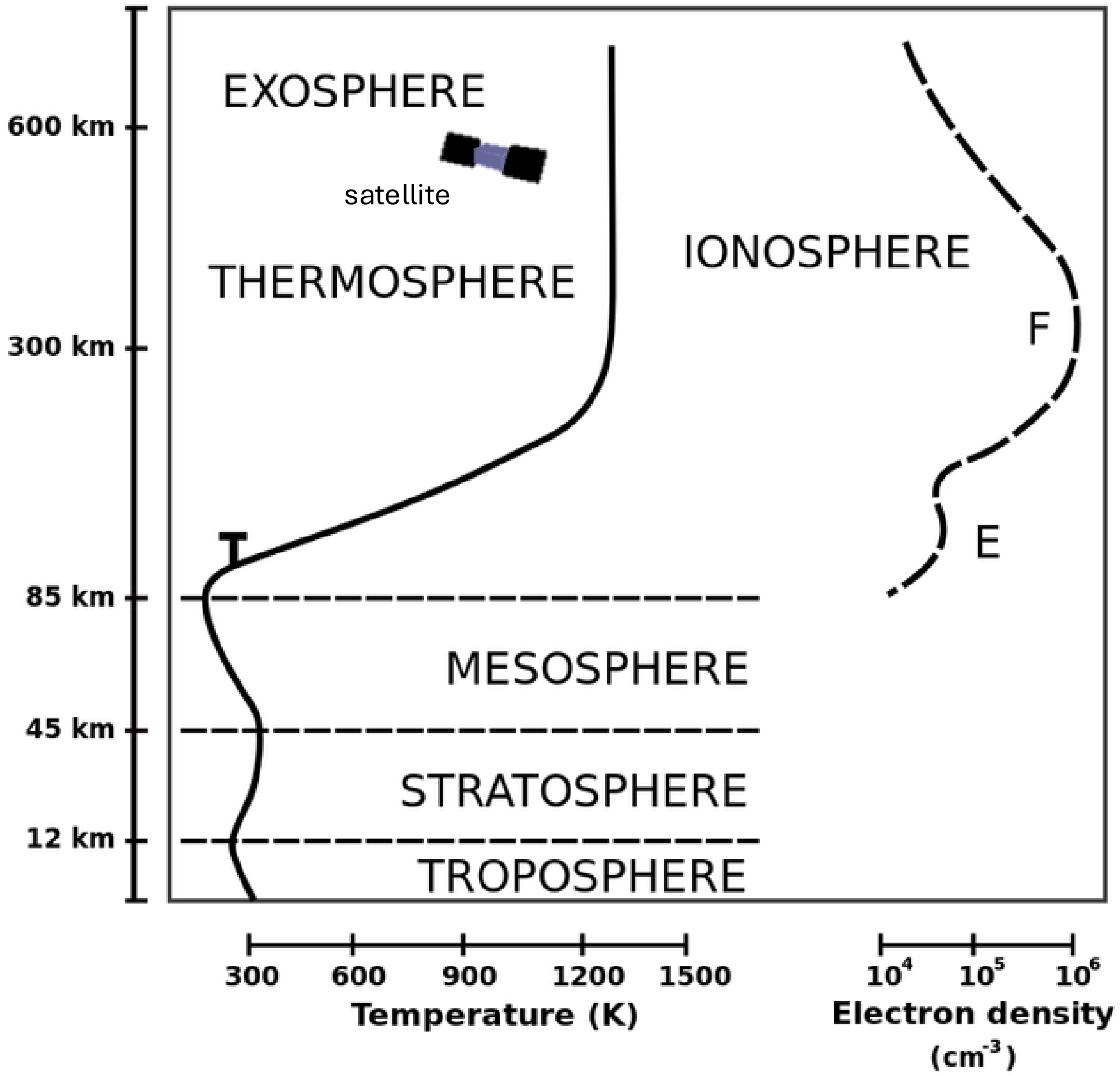

The Earth's Ionosphere

- Extending roughly from 50 km to 1,000 km in altitude, is continuously shaped by solar ultraviolet and extreme ultraviolet radiation (1 – 120 nm), which ionizes the atmospheric gases.
- In addition, events such as solar flares and coronal mass ejections can trigger abrupt changes in electron density and temperature.
- Relative maxima and minima identify the ionospheric regions and layers.
- The ionosphere varies with geographic latitude, longitude, time of the day, season, altitude, magnetic latitude and solar activity.

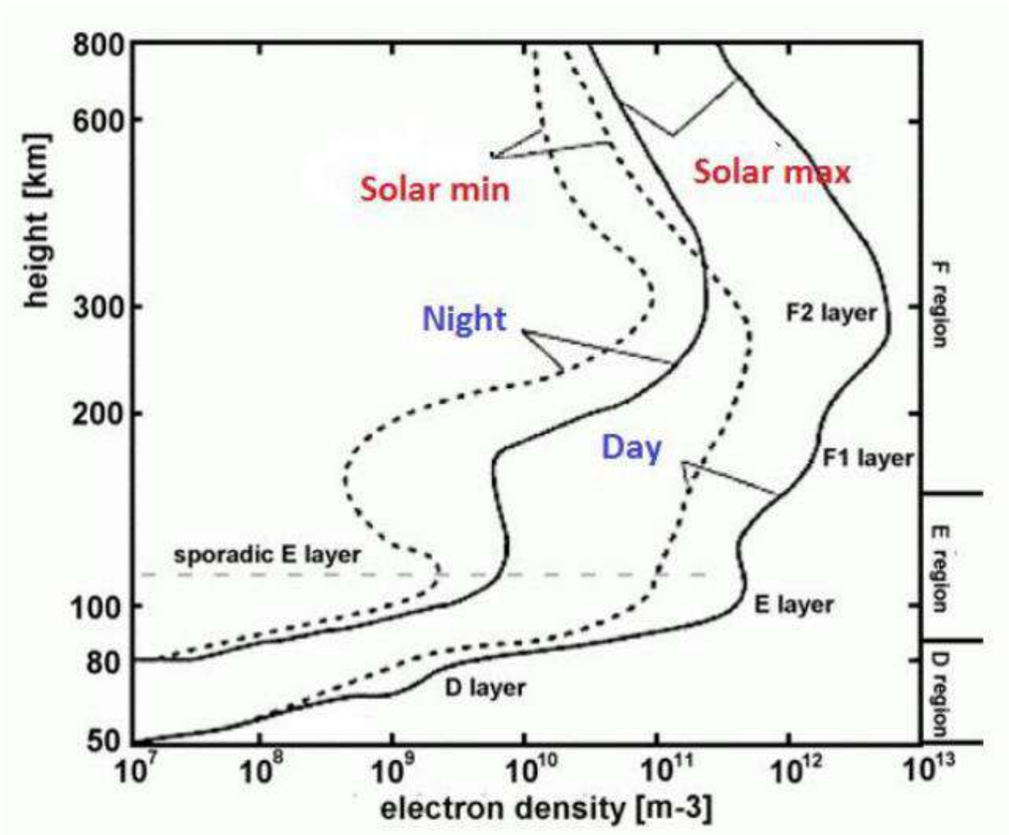

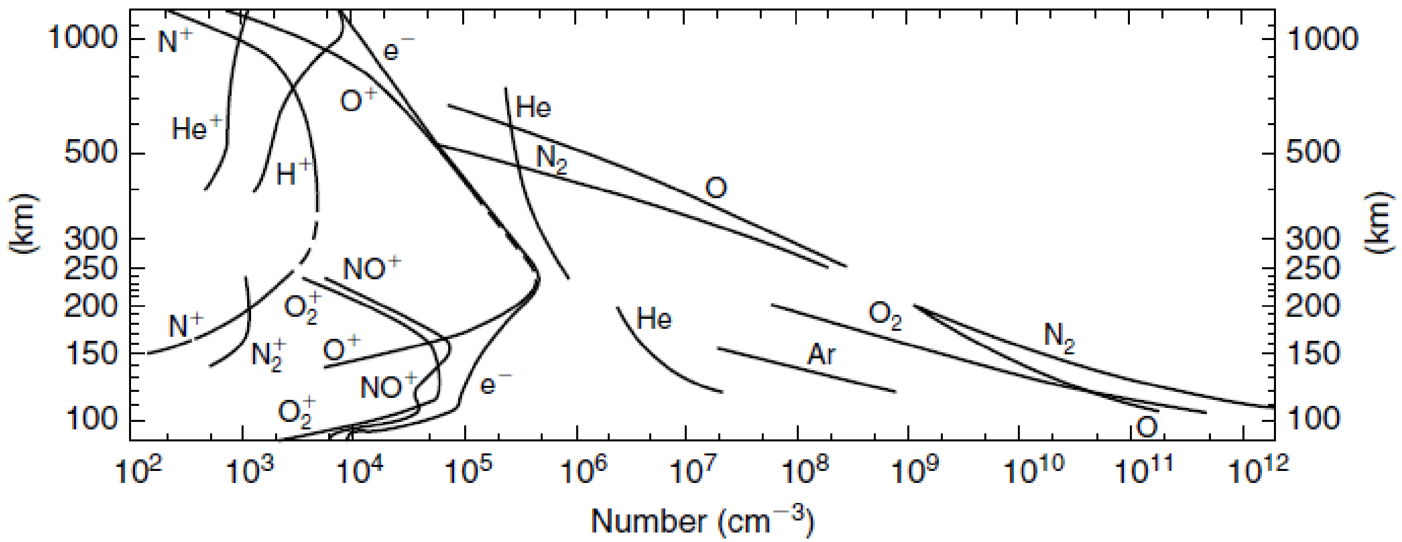

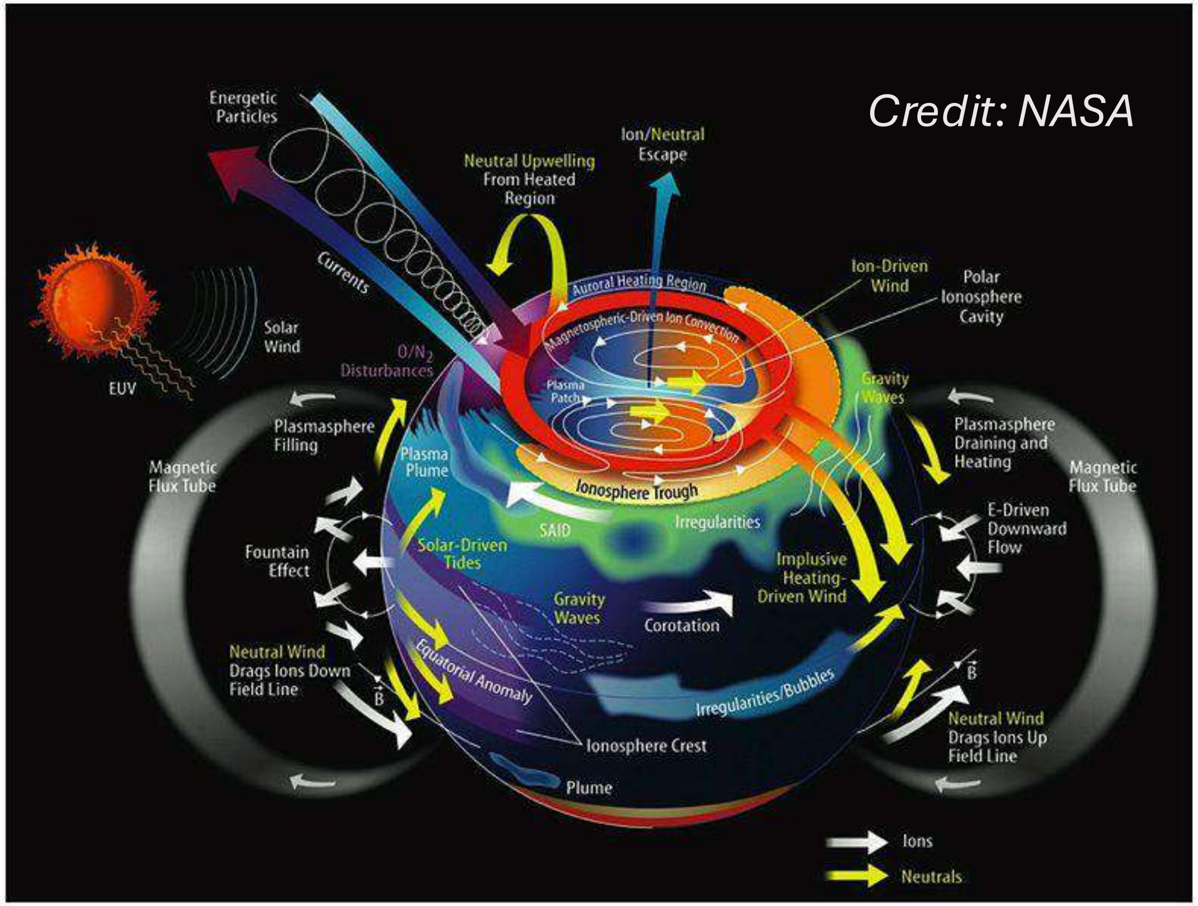

Thermodynamical, dynamical and chemical reactions such as:

- ❖ Neutral composition changes;
- ❖ Changes in the global wind circulation
- ❖ Travelling Atmospheric Disturbances (TADs)

Electrodynamical processes such as:

- ❖ Penetration of electric fields of magnetospheric and interplanetary origin into the ionosphere
- ❖ Enhanced plasma fluxes from the plasmasphere and/or magnetosphere

The Earth's Ionosphere

The Earth's ionosphere is a dynamic plasma environment where solar radiation, geomagnetic forces, and atmospheric processes converge to create a complex system

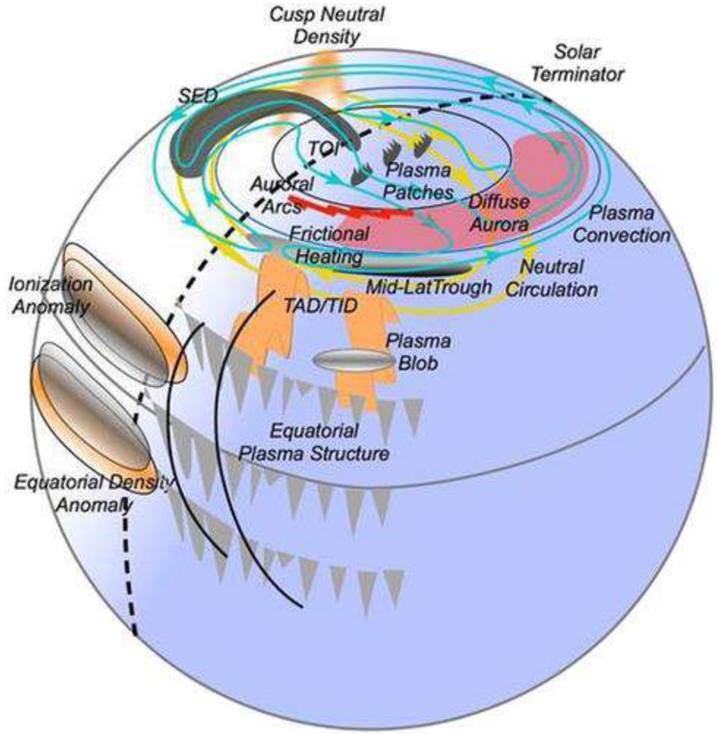

These variations can, in turn, generate or enhance plasma irregularities!

Ionospheric Irregularities

Ionospheric irregularities are disturbances or variations in the ionospheric plasma that can significantly impact radio wave propagation, satellite signals, and other forms of electromagnetic radiation.

The complex and strongly variable plasma dynamics of the Ionosphere may evolve in a wide variety of irregularities with spatial scales ranging from meters to thousands of kilometres, including:

- Sporadic E layer and spread F;
- Field-aligned irregularities (FAIs), and plasma bubbles ;
- Electron density enhancements or depletions
- Traveling ionospheric disturbances (TIDs);
- Conductivity variations;
- Electromagnetic fluctuations in the ULF-ELF bands (1mHz-3 kHz);
- Lightning, whistlers and ELVES;

The formation of irregularities is generally attributed to ionospheric instability mechanisms, including:

- wind shear theory;
- gradient-drift instability;
- atmospheric gravity waves;
- Kelvin-Helmholtz and Rayleigh–Taylor instabilities;

In all the above instability mechanisms, electric fields and neutral winds play dominant roles in the generation of ionospheric irregularities.

Irregularities…what else?

Decoding multiple source signatures in coseismic ionospheric disturbances of the 2024 January M_w7.5 Noto-Peninsula earthquake, Central Japan

Kosuke Heki

Dept. Earth Planet. Sci., Hokkaido Univ., N8 W10, Kita-ku, Sapporo-city, Hokkaido 060-0810, Japan

ARTICLE INFO

Keywords:
2024 Noto-Peninsula earthquake
GNSS-TEC
Coseismic ionospheric disturbance
Slow earthquake
MSTID

ABSTRACT

Vertical crustal movements associated with large earthquakes excite various kinds of atmospheric waves. They propagate upward and often disturb ionosphere. Here, I report a case for the 2024 January 1 M_w7.5 earthquake that occurred in the northern tip of the Noto Peninsula, Central Japan, using a dense network of multi-GNSS receivers. A rectangular-shaped positive anomaly of ionospheric total electron content emerged ~9 min after the mainshock. The initial sharp peak was composed of two acoustic wave pulses excited at the two ends of the fault spanning ~100 km. It was followed by a series of smaller-amplitude broad peaks, the largest of which was possibly excited by a slow fault rupture near the NE edge of the fault ~8 min after the mainshock. These signatures become large where the wavefronts overlap with those of medium-scale traveling ionospheric disturbances, suggesting possible enhancement of the coseismic signals by downward displacements of high electron density regions in the ionosphere.

Journal of Geophysical Research: Space Physics

RESEARCH ARTICLE
10.1002/2013JA019530

On the use of geomagnetic indices and ULF waves for earthquake precursor signatures

J. L. Currie[1] and C. L. Waters[1]

[1]School of Mathematical and Physical Sciences, University of Newcastle, Callaghan, New South Wales, Australia

Key Points:
- Geomagnetic indices are uncorrelated with Pc3 power
- Pc3 power depends on magnetic latitude and local time
- Pc3 spectral ratio is a candidate for a ULF earthquake precursor parameter

Correspondence to:
C. L. Waters,
Colin.Waters@newcastle.edu.au

Citation:
Currie, J. L., and C. L. Waters (2014), On the use of geomagnetic indices and ULF waves for earthquake precursor signatures, *J. Geophys. Res. Space Physics, 119*, 992–1003, doi:10.1002/2013JA019530.

Abstract Ultralow frequency (ULF: 0.001–5 Hz) magnetic records have recently been used in the search for short-term earthquake prediction methods. The separation of local and global effects in the magnetic records is the greatest challenge in this research area. Geomagnetic indices are often used to predict global ULF magnetic behavior where it is assumed that increases in a geomagnetic index correspond with an increase in ULF power. This paper examines the relationships between geomagnetic indices and ULF power, spectral polarization ratio, and the relationship between the spectral polarization ratio and solar wind parameters. The power in the ULF, Pc3-5 bands (10–600 s), shows a linear correlation coefficient of 0.2 with the *Kp* magnetic activity index. The correlation varies with magnetic local time (MLT) and latitude. The correlation coefficient is inversely related to the integrated power in the ULF Pc3 band (10–45 s) over MLT and magnetic latitude. The ratio of spectral powers $Z(\omega)/G(\omega)$ is discussed and shown to be a promising parameter in the search for earthquake precursor signals in ULF records.

IONOSPHERIC SIGNATURES OF SEISMIC EVENTS AS OBSERVED BY THE DEMETER SATELLITE

M. Parrot and F. Lefeuvre
LPC2E/CNRS, 3 A Av Recherche Scientifique
45071 Orleans cedex 2 France
lefeuvre@cnrs-orleans.fr

URSI

KEYWORDS: seismic activity, ionospheric signatures, EM wave field perturbations, ion density perturbations, electron density perturbations

ABSTRACT:

Observations made by the CNES/DEMETER satellite, from March 2004 to December 2010, are used to evaluate the efficiency of ionospheric signatures of seismic events. Ionospheric signatures are defined. They are applied to observations made for a series of Chile earthquakes including the 27 February 2010 one (M 8.8). Case studies and statistical studies are used to point out precursor signals. Points to be solved to get reliable precursory signals are discussed.

Examples of unusual ionospheric observations made by the DEMETER satellite over seismic regions

M. Parrot [a,*], J.J. Berthelier [b], J.P. Lebreton [c], J.A. Sauvaud [d], O. Santolík [e], J. Blecki [f]

[a] LPCE/CNRS, 3A Avenue de la Recherche Scientifique, 45071 Orléans cedex 2, France
[b] CETP, Observatoire de Saint Maur, 4 Avenue de Neptune, 94107 Saint Maur des Fossés cedex, France
[c] Research and Scientific Support department, ESA/ESTEC, Noordwijk, The Netherlands
[d] CESR/CNRS, 9 avenue du Colonel Roche, 31028 Toulouse cedex 4, France
[e] Charles University, Faculty of Mathematics and Physics, Prague, Czech Republic
[f] Space Research Centre PAS, Bartycka 18A, 00-716 Warsaw, Poland

ELSEVIER

Accepted 6 February 2006
Available online 19 May 2006

Abstract

The micro-satellite DEMETER was launched on June 29, 2004 in a polar and circular orbit with an altitude of ~710 km. It is a CNES mission controlled from Toulouse in France. The main objective of DEMETER is to search and characterize ionospheric perturbations that can be associated with the seismic activity in order to better understand the generation mechanism of such perturbations. Its scientific payload allows us to measure waves in a broad frequency range and also some important plasma parameters (ion composition, electron density and temperature, energetic particles). This paper is a preliminary report of unusual observations recorded by DEMETER over seismic regions prior to earthquakes. The main purpose of the project is to perform a statistical analysis with many events in order to determine the necessary conditions to observe such seismo-electromagnetic effects. It is too early to perform such statistics but data recorded during selected events and shown here are useful since they may point out sensitive parameters which must be particularly surveyed in the statistical analysis.

Keywords: Ionosphere; Seismic activity; DEMETER

JGR Space Physics

RESEARCH ARTICLE
10.1029/2020JA028709

Key Points:
- Distinct effects of various seismic

Association of Ionospheric Signatures to Various Tectonic Parameters During Moderate to Large Magnitude Earthquakes: Case Study

A. S. Sunil[1], Mala S. Bagiya[1], Quentin Bletery[2], and D. S. Ramesh[1]

[1]Indian Institute of Geomagnetism (DST), Navi Mumbai, India, [2]Université Côte d'Azur, IRD,CNRS, Observatoire de la Côte d'Azur, Géoazur, Valbonne, France

Abstract The sudden ground movement associated with Mw > 6.5 earthquakes is considered a potential source of ionospheric electron density perturbations over the fault region. Coseismic ground displacement is a function of various seismic source parameters such as moment magnitude, focal depth, and focal mechanism etc. We study here the distinct effects of vertical ground displacement, moment magnitude and focal depth on coseismic ionospheric perturbation (CIP) amplitudes during moderate-to-large earthquakes. We analyze GPS-total electron content variations during 59 dip-slip earthquakes that occurred in the last 20 years. Our study reveals that though CIP amplitudes are primarily controlled by moment magnitude, they are also sensitive to the earthquake focal depth. To understand the influence of focal depth on the displacement field and therefore on CIP amplitudes, we present a simple synthetic test, for a depth range of 0–200 km, highlighting that the maximum vertical ground displacement decreases logarithmically with increasing focal depth while the volume (i.e., integrated vertical ground displacement) of uplifted/subsided material varies very marginally. We conclude that CIP is sensitive to the wavelength of co-seismic vertical displacement field and that seismic energy propagation to the overlying atmosphere during deep earthquakes is not adequate to generate detectable CIP.

Seismogenic ULF/ELF Wave Phenomena: Recent Advances and Future Perspectives

Masashi Hayakawa[1,2*], Alexander Schekotov[3], Jun Izutsu[4], Alexander P. Nickolaenko[5], Yasuhide Hobara[6]

[1]Hayakawa Institute of Seismo Electromagnetics Co. Ltd. (Hi-SEM), UEC Alliance Center #521, Tokyo, Japan
[2]The University of Electro-Communications (UEC), Advanced & Wireless Communications Research Center (AWCC), Tokyo, Japan
[3]Institute of Physics of the Earth, Russian Academy of Sciences, Moscow, Russia
[4]Chubu University, International Digital Earth Applied Science Research Center, Kasugai Aichi, Japan
[5]Usikov Institute for Radio-Physics and Electronics, National Academy of Sciences of the Ukraine, Kharkov, Ukraine
[6]UEC, Graduate School of Informatics and Engineering, Tokyo, Japan
Email: *hayakawa@hi-seismo-em.jp, hayakawa@hi-seismo-em.jp, my@aschekotov.ru, izutsu@isc.chubu.ac.jp, sashanickolaenko@gmail.com, hobara@ee.uec.ac.jp

How to cite this paper: Hayakawa, M., Schekotov, A., Izutsu, J., Nickolaenko, A.P. and Hobara, Y. (2023) Seismogenic ULF/ELF Wave Phenomena: Recent Advances and Future Perspectives. *Open Journal of Earthquake Research*, 12, 45-113.
https://doi.org/10.4236/ojer.2023.123003

Received: April 4, 2023
Accepted: June 6, 2023
Published: June 9, 2023

Abstract

There has been enormous progress in the field of electromagnetic phenomena associated with earthquakes (EQs) and EQ prediction during the last three decades, and it is recently agreed that electromagnetic effects do appear prior to an EQ. A few phenomena are well recognized as being statistically correlated with EQs as promising candidates for short-term EQ predictors: the first is ionospheric perturbation not only in the lower ionosphere as seen by sub-ionospheric VLF (very low frequency, 3 kHz < f < 30 kHz)/LF (low frequency, 30 kHz < f < 300 kHz) propagation but also in the upper F region as detected by ionosondes, TEC (total electron content) observations, satellite observations, etc, and the second is DC earth current known as SES (Seismic electric signal). In addition to the above two physical phenomena, this review highlights the following four physical wave phenomena in ULF (ultra low frequency, frequency < 3 Hz)/ELF (extremely low frequency, 3 Hz < frequency < 3 kHz) ranges, including 1) ULF lithospheric radiation (*i.e.*, direct radiation from the lithosphere), 2) ULF magnetic field depression effect (as an indicator of lower ionospheric perturbation), 3) ULF/ELF electromagnetic radiation (radiation in the atmosphere), and 4) Schumann resonance (SR) anomalies (as an indicator of the perturbations in the lower ionosphere and stratosphere). For each physical item, we will repeat the essential points and also discuss recent advances and future perspectives. For the purpose of future real EQ prediction practice, we pay attention to the statistical correlation of each phenomenon with EQs, and its predictability in terms of probability

"To be able to distinguish the ionospheric precursors from the other kinds of ionospheric variability it is necessary to know their main morphological features."

Pulinets, S., & Boyarchuk, K. (2004). *Ionospheric precursors of earthquakes*. Springer Science & Business Media.

Ionospheric studies in the frame of Scienza +

AIM: Distinguishing between naturally occurring disturbances—driven by solar and geomagnetic activity—and those potentially induced by seismic events

HOW: Investigating the intricate behaviors of the ionosphere in terms of:

- Identification of instrumental and environmental background;
- Characterization of ionospheric irregularities;
- Characterization of particle acceleration mechanisms;
- Identification and characterization of ULF and ELF waves;
- Characterization turbulent variations in electric and magnetic fields;
- Calculation of ionospheric electrical conductivity;
- Modeling of the topside ionosphere;

This knowledge is key to enhance our ability to assess potential lithosphere-atmosphere-ionosphere coupling mechanisms.

The ionospheric background

Step 1 – Selection of the geographical region

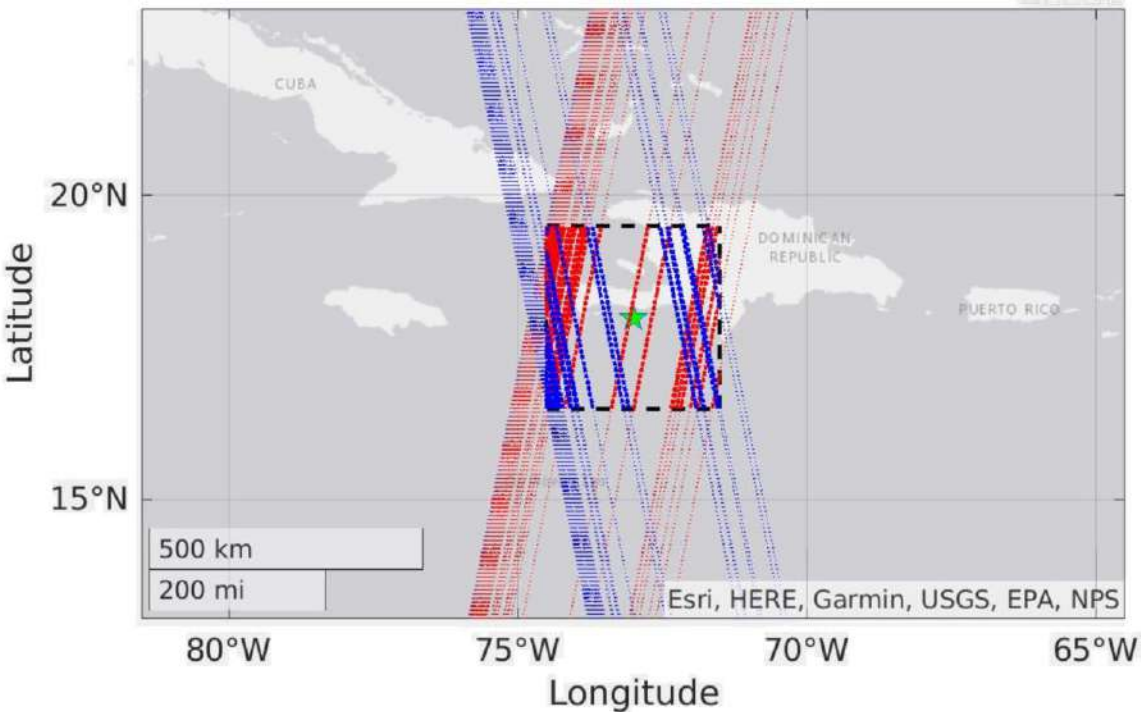

Diurnal orbits Nocturnal orbits

The considered orbits are enclosed in a $3^\circ \times 3^\circ$ geographic LAT-LON cell cantered on the EE.

edge effects

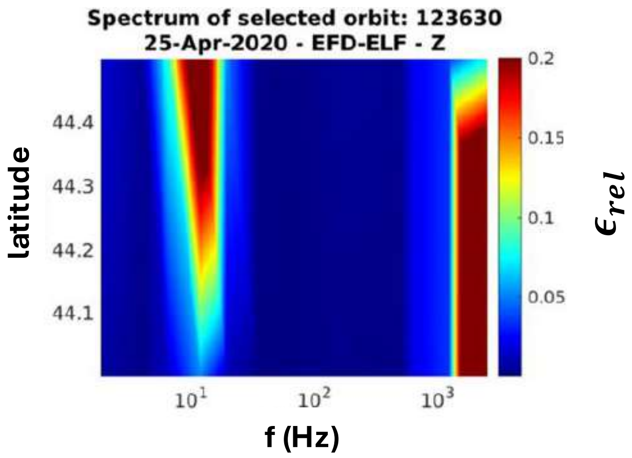

Step 2 – Decomposition of the selected signals

Fast Iterative Filtering (FIF)*

Similarly to EMD, FIF decomposes the signal into intrinsic mode components (IMC).

$$f(t) = \sum_{l=1}^{N} IMC_l(t) + r(t)$$

*Cicone, A., Zhou, H. Numerical analysis for iterative filtering with new efficient implementations based on FFT. *Numer. Math.* 147, 1–28 (2021).

The ionospheric background

Step 3 – Multiscale statistical analysis and ϵ_{rel} evaluation

$$\epsilon_{rel}(l) = \frac{\int_l |IMC_l(t)|^2 \, dt^*}{\int_l |f(t)|^2 \, dt}$$

Relative energy of the single IMF divided by the total energy calculated in the interval chosen for the PDF calculation.

*Flandrin, P. (1998). Time-frequency/time-scale analysis. Cambridge, Massachusetts: Academic Press.;

Step 4 – calculation of latitude-frequency-ϵ_{rel} spectrum

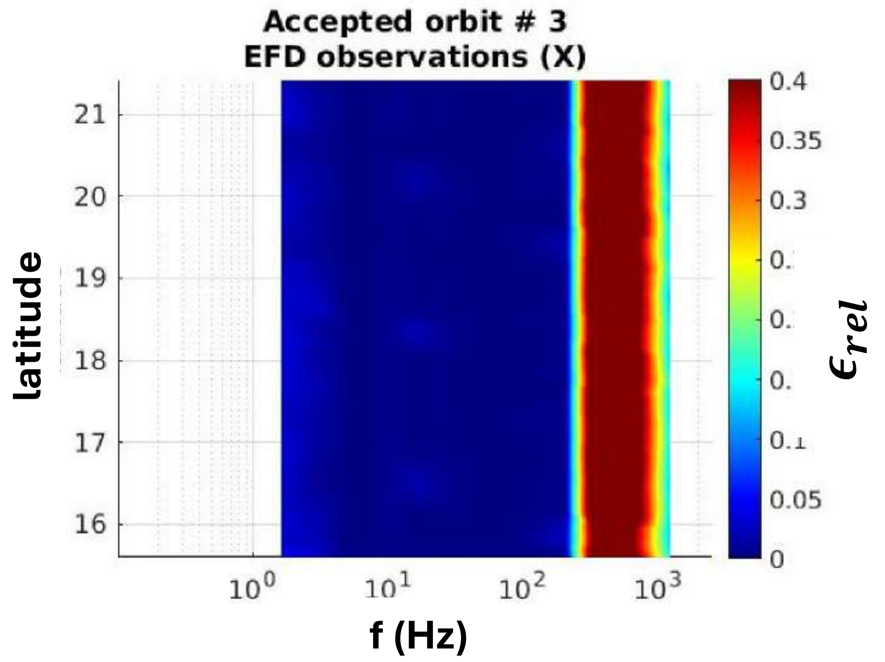

The ionospheric background

Step 5 – Remapping

Every spectrum has different grid values both in latitudes and frequencies

Constructing a grid on which remap the whole dataset

Latitudes

Linear spacing
from $lat_C - L_G/2$ to $lat_C + L_G/2$
with 0.1° spacing

Frequencies

Logarithmic spacing
since frequency values span several orders of magnitude

Final uniform grid for every orbits with ϵ_{rel} interpolated on every grid point

Step 6 – Average

The Background is defined as the average of all the ϵ_{rel} remapped on the final grid

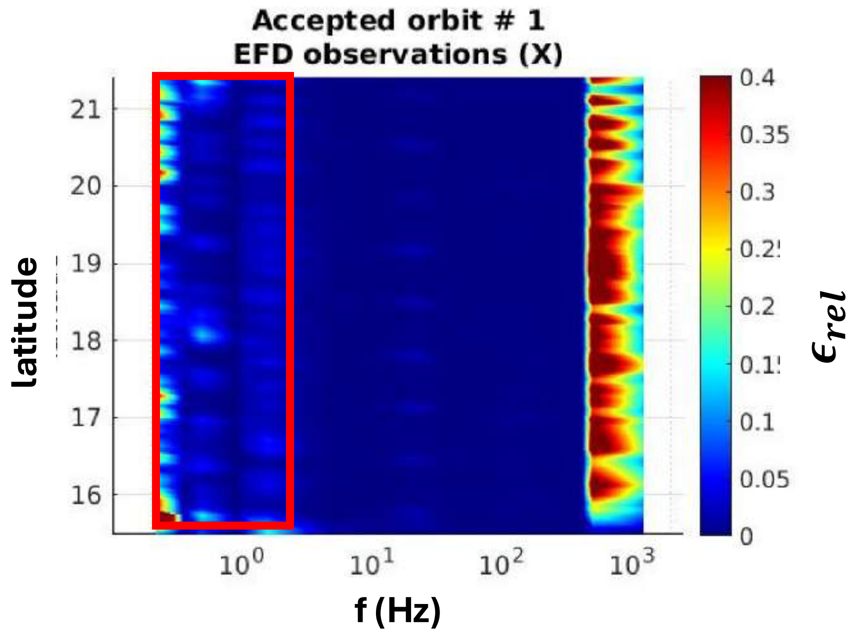

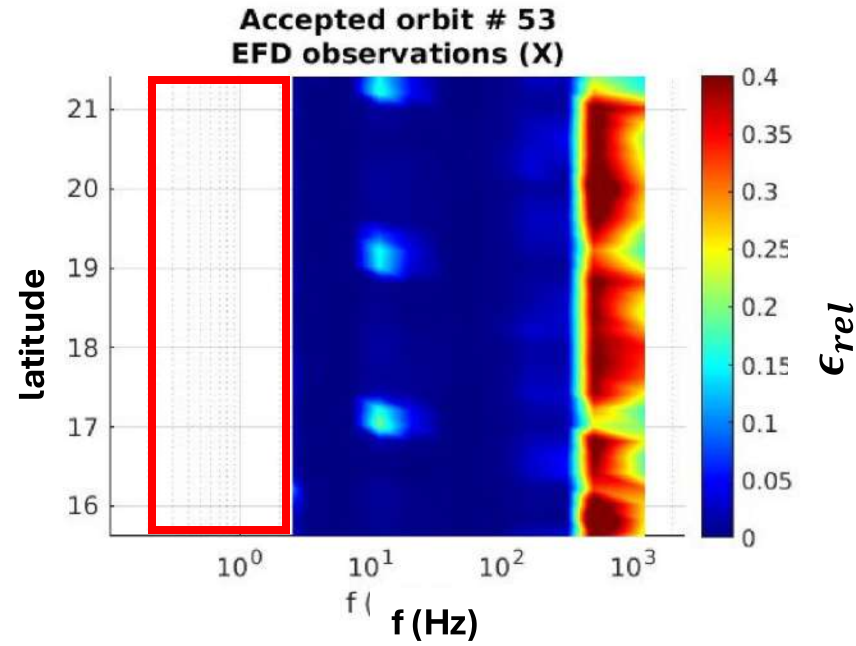

First automatized procedure to characterize the ionospheric EM background

9 different backgrounds to **consider all the possible ionospheric conditions**

Vanuatu Island

ALL

QUIET

DIST.

- **2 Hz:** $\vec{v} \times \vec{B}$ electric field caused by satellite motion into the geomagnetic field
- **8-15 Hz:** Schumann resonances at CSES orbit
- **1 kHz:** Plasmaspheric hiss

DAY & NIGHT

DAY

NIGHT

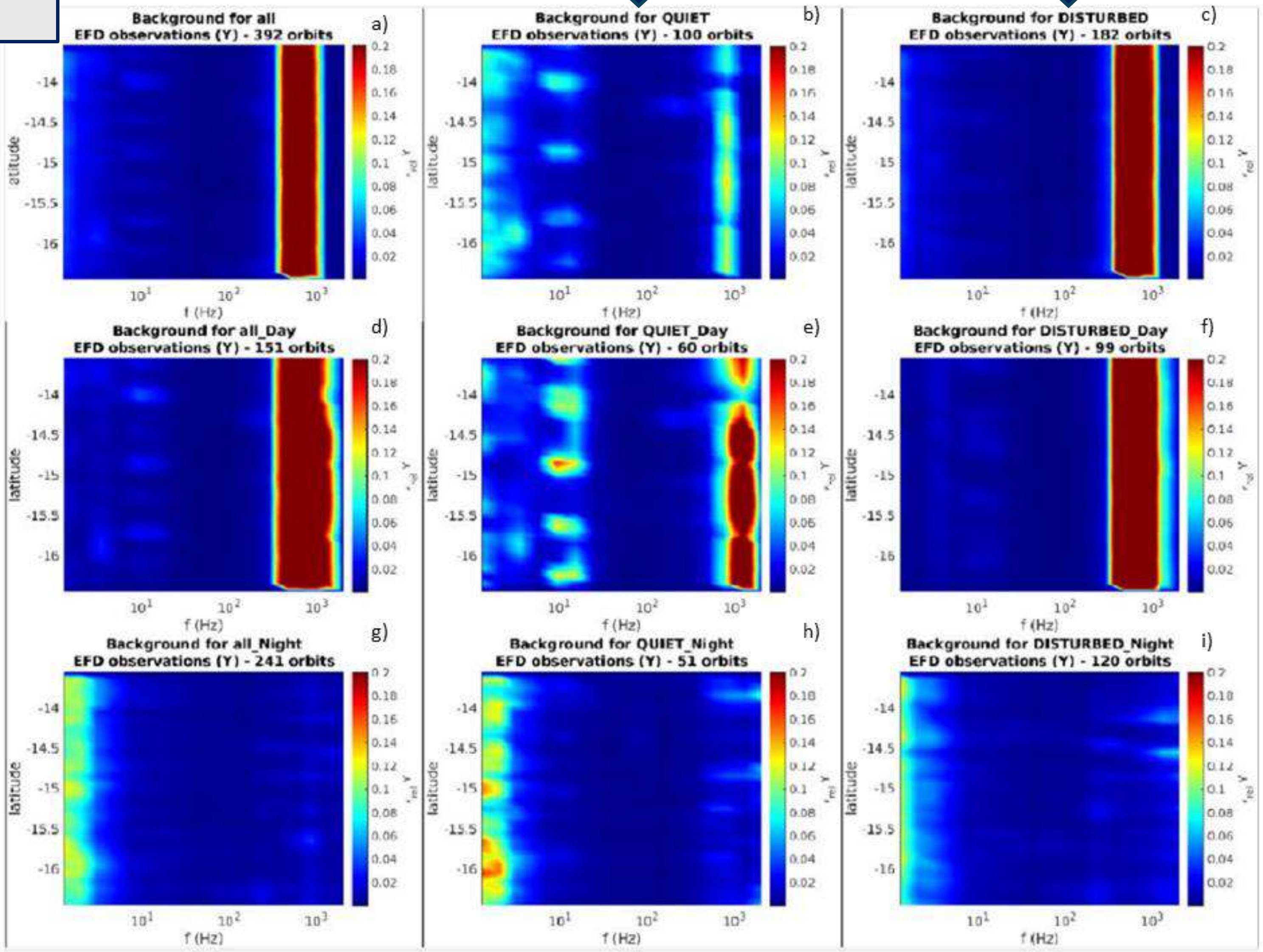

The generated backgrounds correctly identify well-known signals in the ionosphere

effectiveness of technique confirmed!

The ionospheric background

Background for Haiti

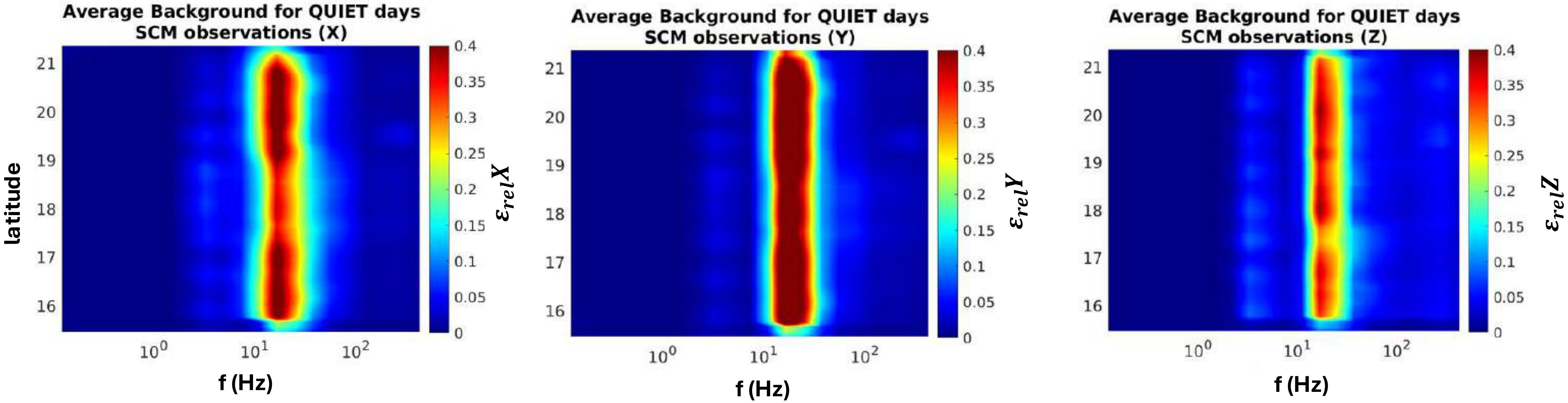

Observations around Haitian earthquake of August 14, 2021 ($M_W = 7.2$)

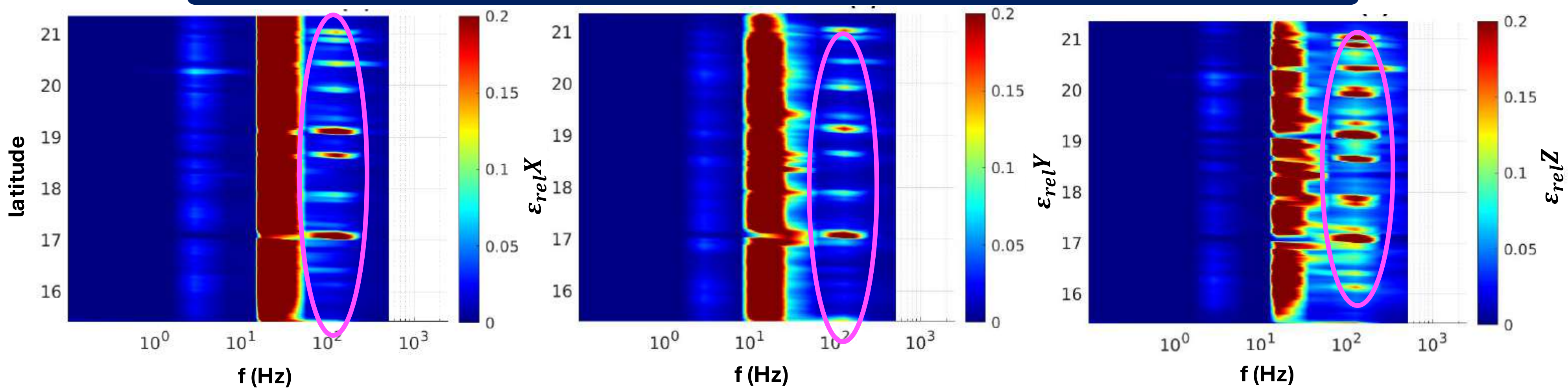

8-15 Hz: Schumann resonances at CSES orbit

Signal emerging from background ~190 Hz

The ionospheric background

Haiti
190 Hz

Vanuatu
400 Hz

All signals are found both in the electric and magnetic field, exhibiting the characteristics of an EM wave

$$\vec{E} \perp \vec{B}$$

Recchiuti et al. (2023)

Indonesia
180 Hz

Italy
80 Hz

EM background could be used to detect electromagnetic seismo-associated signature!!

Characterization of low latitude irregularities

WHY LOW LATITUDES?

1°

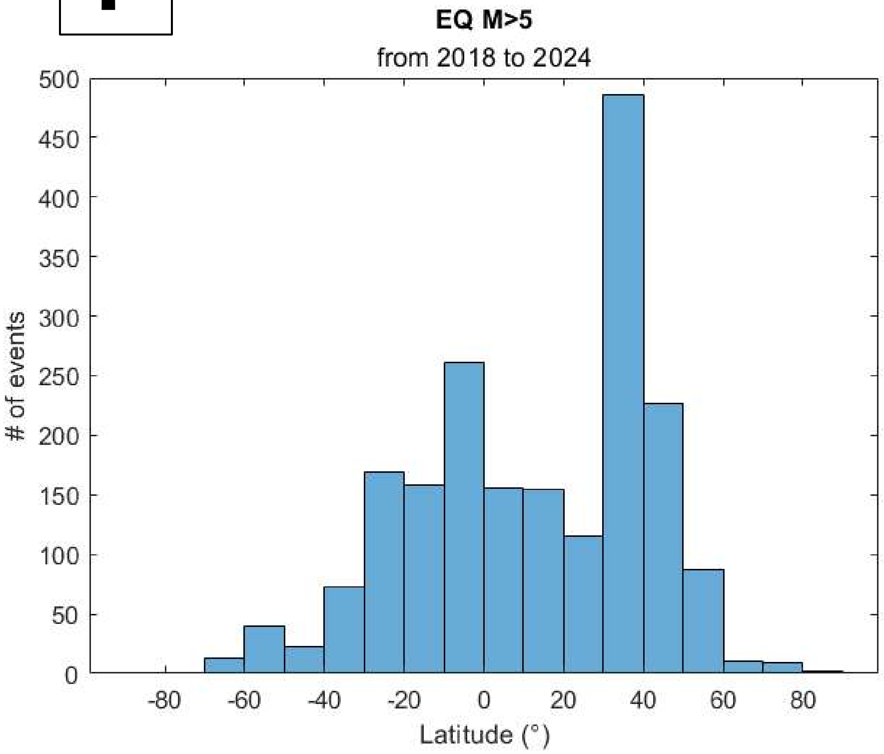

2°

The ionosphere over the Equatorial Region/low latitudes possesses **features** that are distinct from those of other latitudes, because of:

- **the horizontal/low inclination geomagnetic field lines** that connect/couple the equatorial F region to its conjugate E layer;
- **the relatively larger fraction the solar radiant energy absorbed** as compared to other latitudes (50% of the total incident solar radiation on Earth is absorbed within ±30 latitude zone cantered on the equator);

The resulting *vertical plasma transport/motion* by dynamo zonal electric field is mainly responsible for the formation and structuring of the ionization layers, and for the over all phenomenology of the equatorial and low latitude ionosphere, such as **the plasma instabilities/irregularities of the night ionosphere**.

Characterization of low latitude irregularities

PLASMA BUBBLES

Plumes of low-density plasma

Generically appear at **local dusk** where the absence of sunlight leads to a much faster ionospheric recombination at lower altitudes with respect to higher ones, thus causing steep upward plasma density gradients which in turn result in growth of the collision-dominated Rayleigh–Taylor (R–T) instability

Such kind of process triggers the formation of plasma-depleted regions in the bottom side of the F-layer, which then buoyantly rise upward into the topside of the F-layer

Traditional diagnostic methods (e.g. GNSS, radars, airglow imagers) allowed to assess the main mechanisms for generating **POST-SUNSET** plasma bubbles, including their multi-scale temporal variability, such as long-term variability mainly due to solar cycle dependences and medium-term variability mainly due to seasonal variations

However, mechanisms generating the **POST-MIDNIGHT** plasma bubble are still unknown and extensively debated.

CSES-01 orbital plane allows to contribute to the study of these irregularities

Characterization of low latitude irregularities

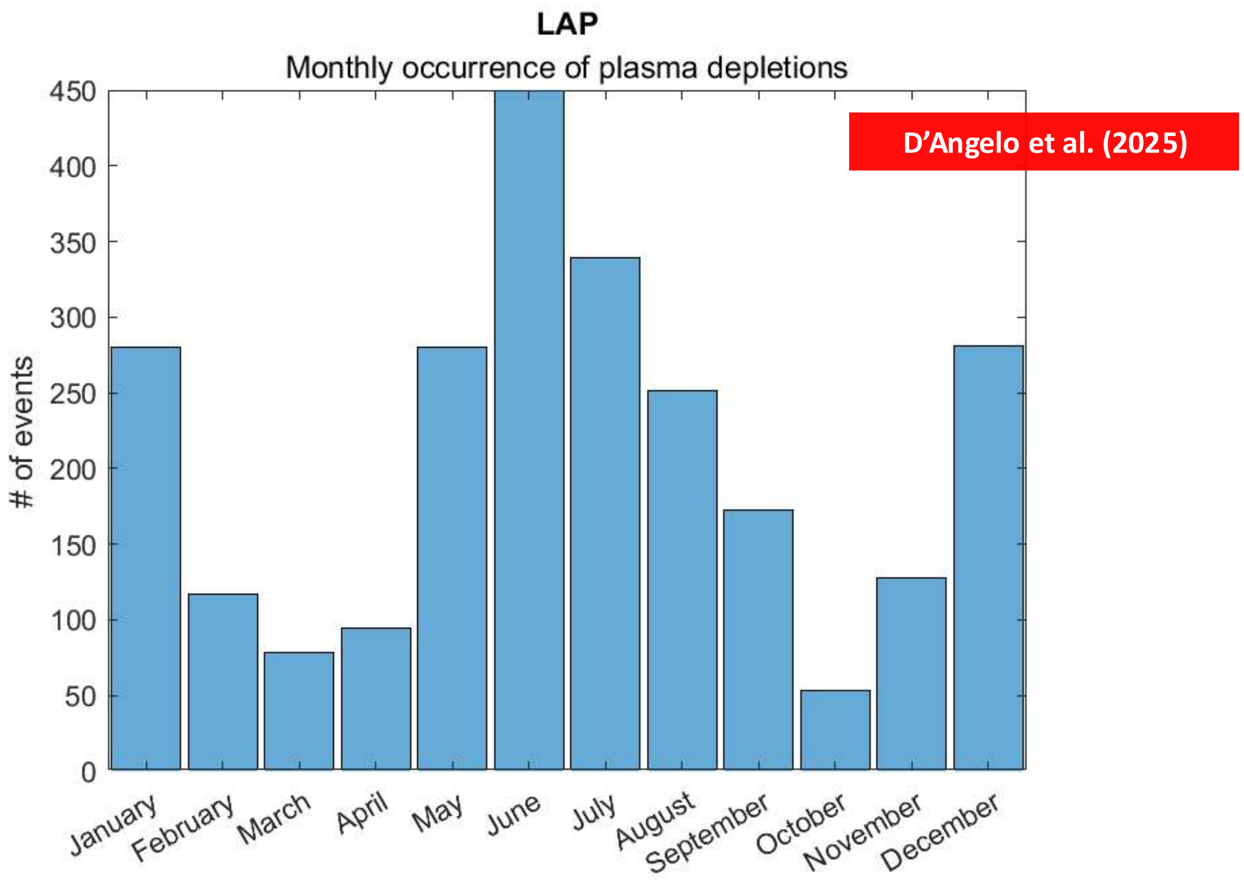

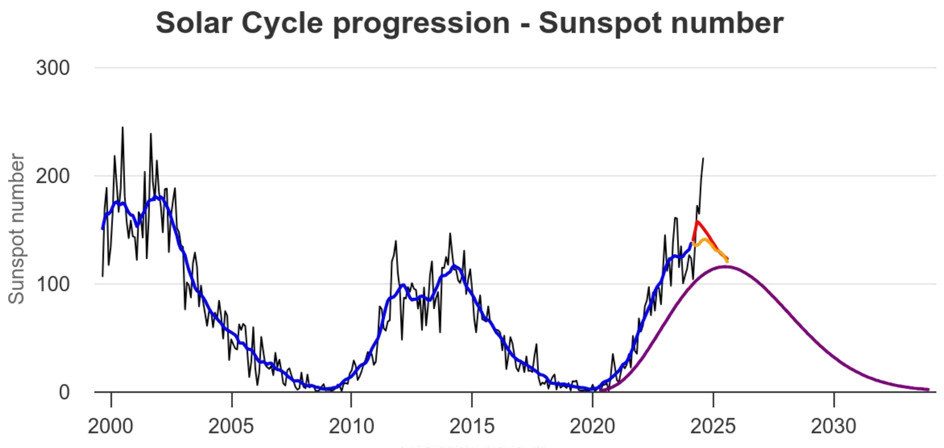

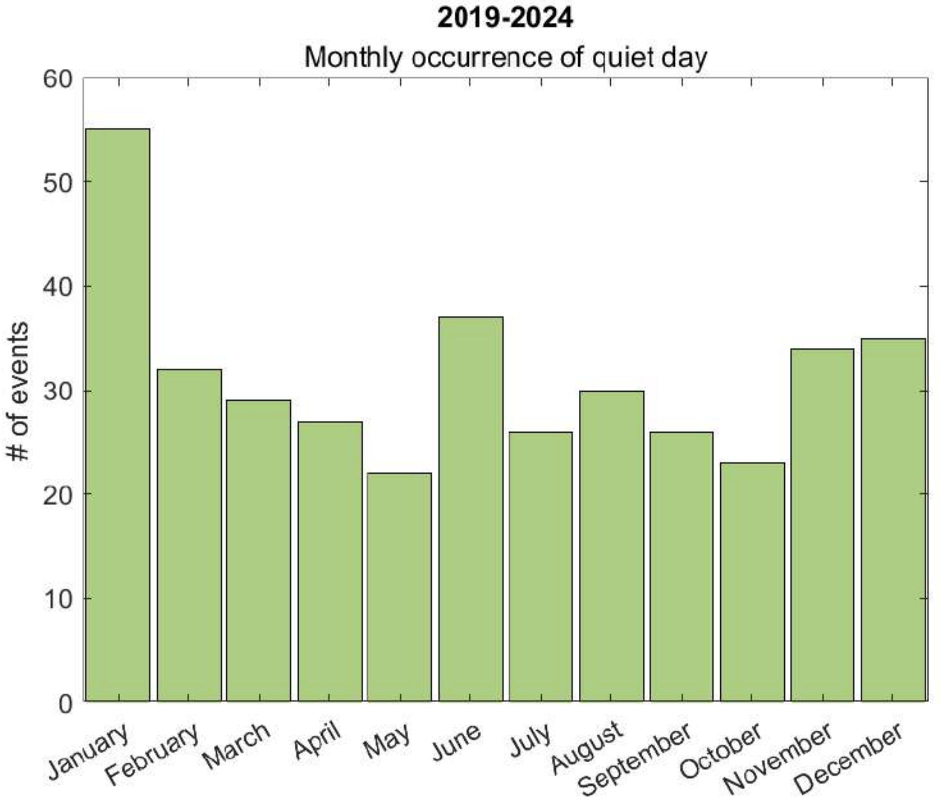

The maximum in the occurrence rate of irregularities across midnight into the post-midnight hours takes place during the June and December solstices, with a peak, during quiet periods, between May and August

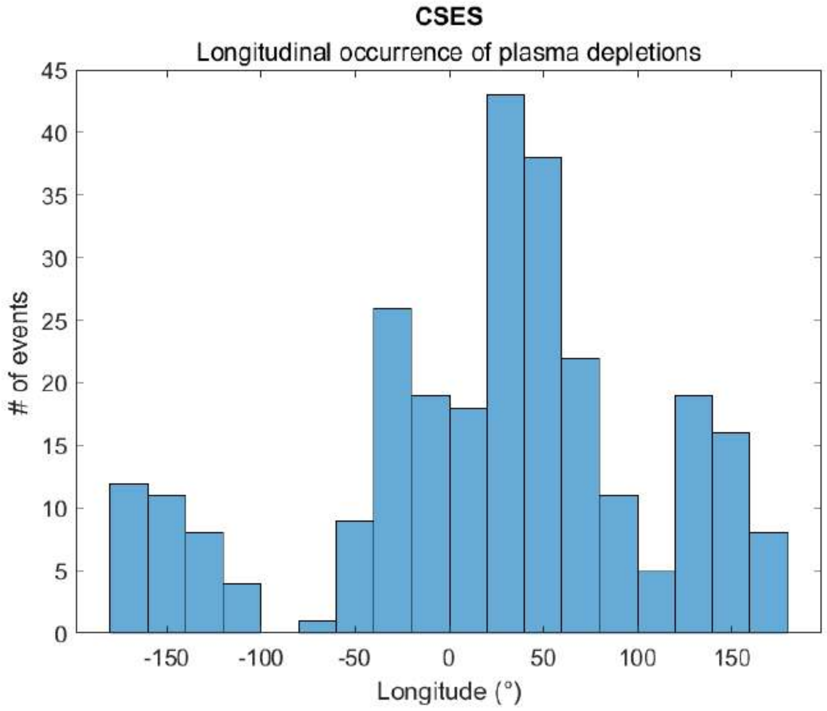

Yizengaw et al. (2013) noted that a strong occurrence of the post-midnight irregularities peak predominantly in the African sector appears during the June solstice suggesting that the abundant appearance of the ionospheric sporadic E layer (Es) in the June solstice could be a source of eastward electric field that leads to bubble formation during the local time after midnight.

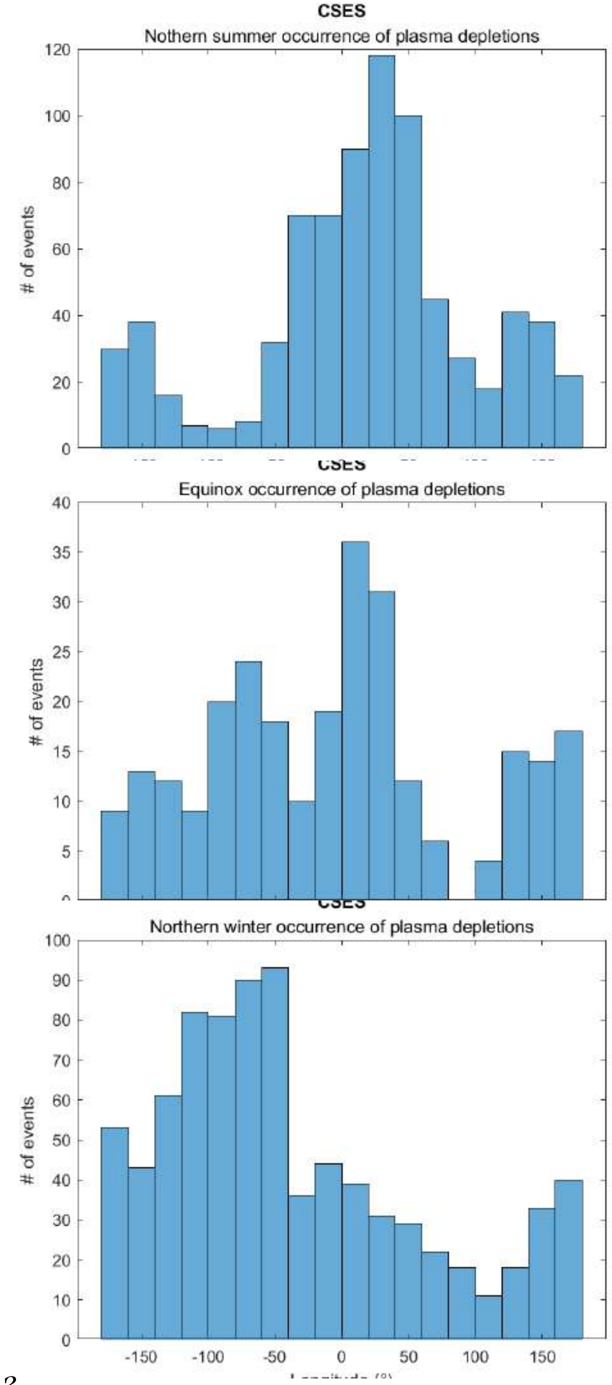

Yizengaw et al., *Geophys Res Lett,* 40, 2013

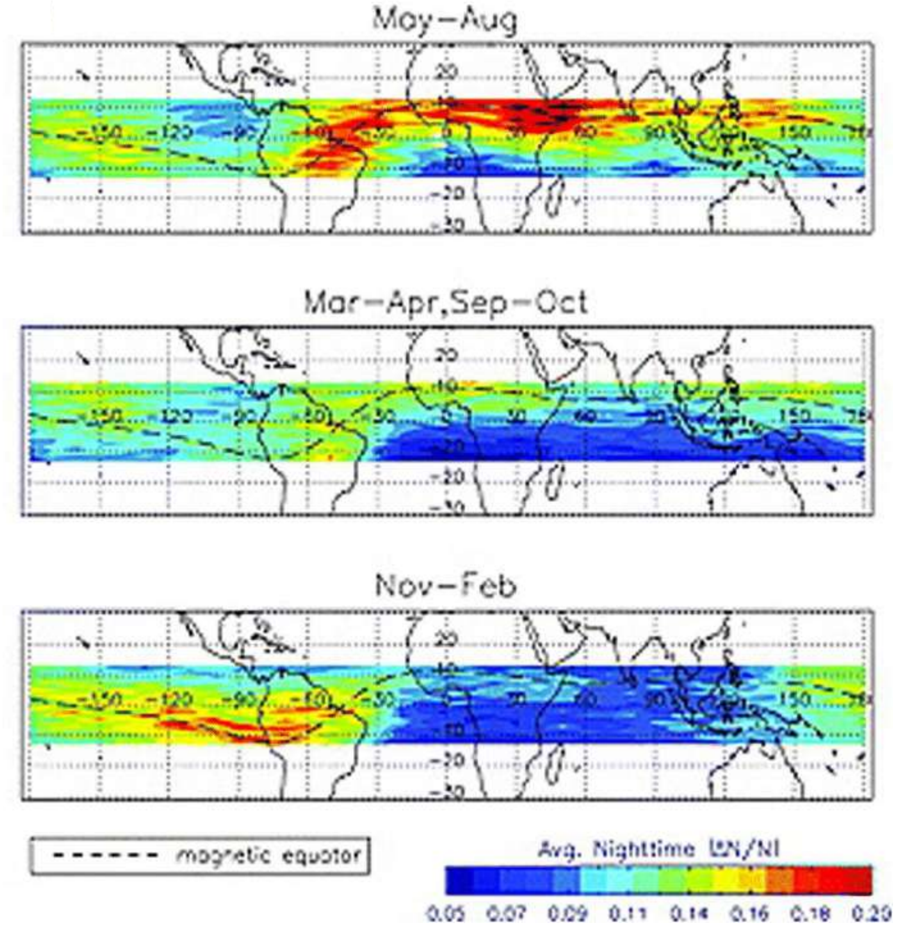

The longitudinal structures in which these irregularities occur are very similar to those reported by Dao et al. (2011), suggesting that the lower atmospheric tides may have actively contributed to EPBs formations.

Dao et al., *Geophys Res Lett*, 38:L10104, 2011

Dynamics of low latitude irregularities

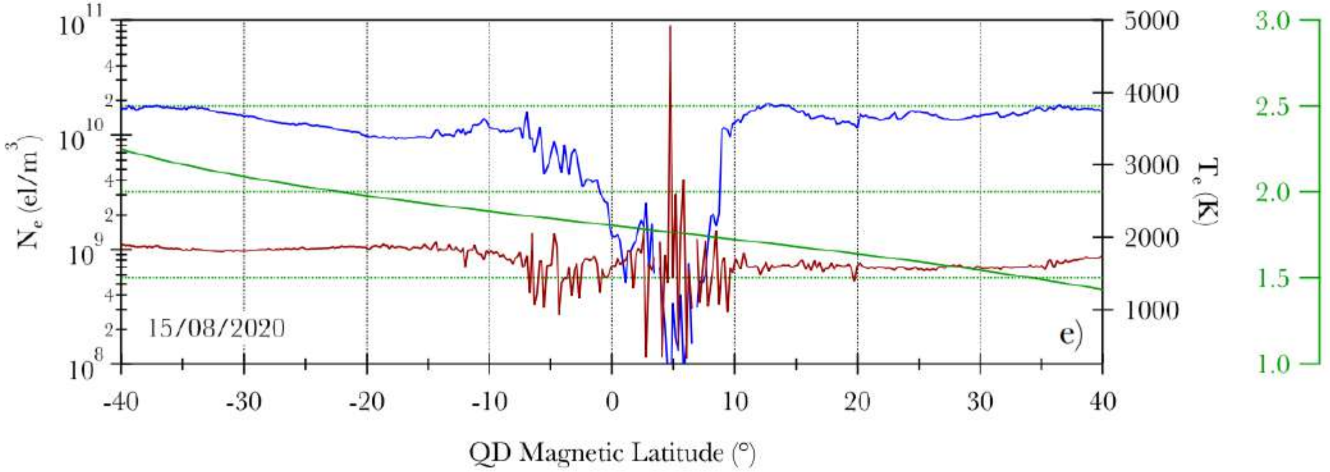

De Michelis et al. (2024)

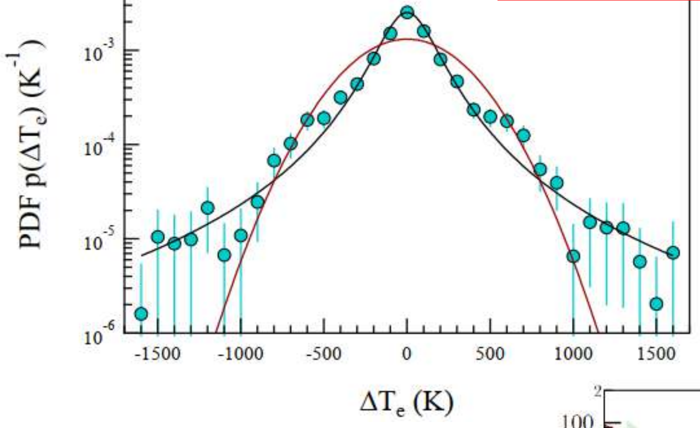

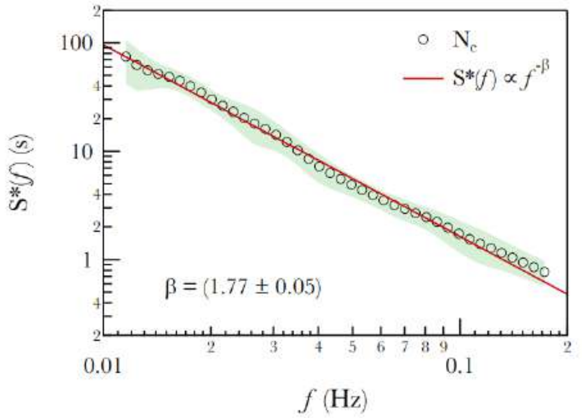

The statistical analysis of a sample of EPBs in geomagnetic quiet conditions revealed

- The multiscale turbulent nature of the electron density fluctuations,
- An electron temperature variability likely connected to compression and expansion of EPBs as they rise and evolve.
- Electron pressure and density have different spectral properties.

New implications for EPBs dynamics:

- development of plasma depletions follows a cascade process like that observed in classical fluid turbulence generated by Raileigh-Taylor instability
- Non negligible thermal effects challenge the one-to-one correspondence of density and magnetic fluctuations invoked for the diamagnetic effect.

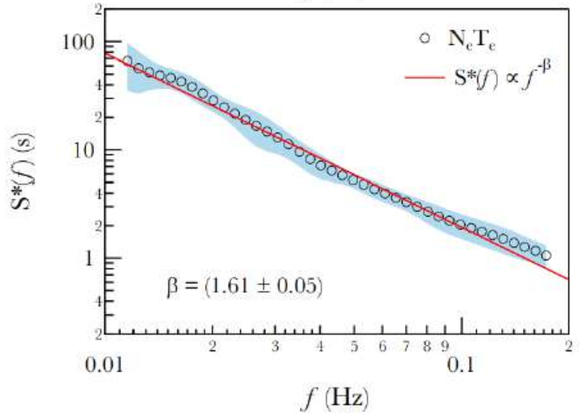

Dynamics of low latitude irregularities

characterization of the ionospheric background electric field due to equatorial ionospheric convection

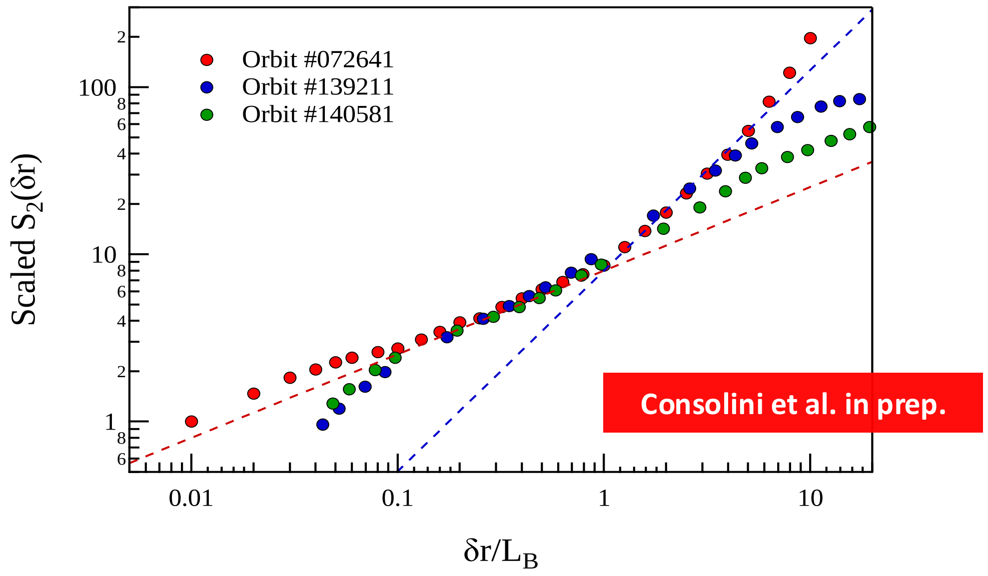

Ionospheric **E x B velocity** drift in Equatorial Plasma Bubbles revealed:

- Coexistence of a 2D large scale convective structures (Bolgiano scaling) with a 3D small-scale (Kolmogorov) turbulence.
- Identification of the scale L_B of the transition between these two regimes, denoting the change in the dominant force (buoyancy or inertial).

Summary: Our results support findings of previous studies and suggest that possible mechanisms for generating observed post-midnight irregularities could be both attributed to the seeding of the Rayleigh–Taylor instability by atmospheric gravity waves (propagating from below into the ionosphere) and, subsequently, to the uplift of the F layer induced by the meridional neutral winds in the thermosphere.

The proposed studies, which represent a **first step towards a broader characterization of low-latitude ionospheric irregularities**, are fundamental to better understand and characterize ionospheric irregularities thus **increasing our ability to assess potential lithosphere-atmosphere-ionosphere coupling mechanisms**

Detection of ionospheric irregularities

D’Angelo et al. (2025) under rev

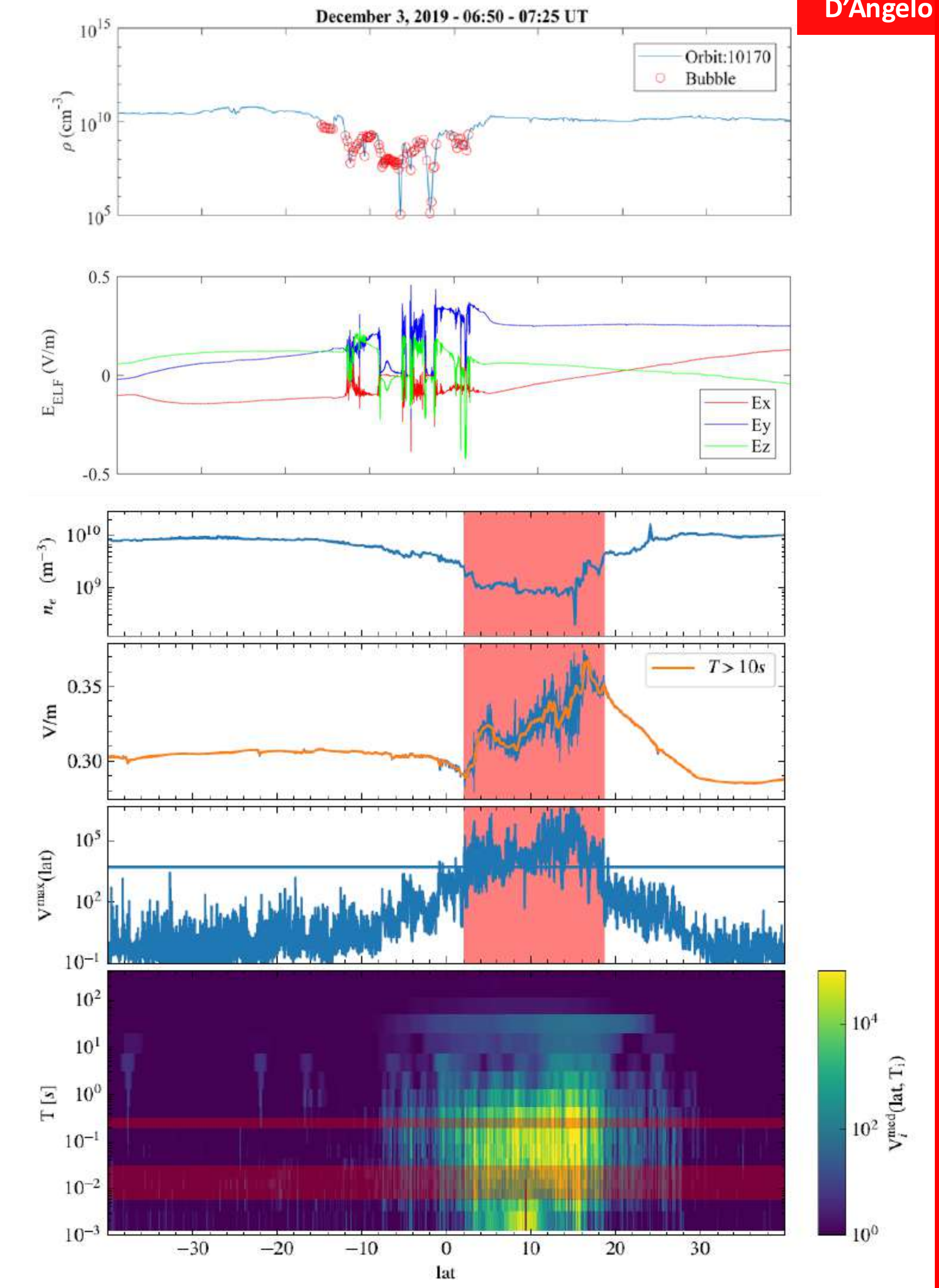

Pezzopane et al. (2022)

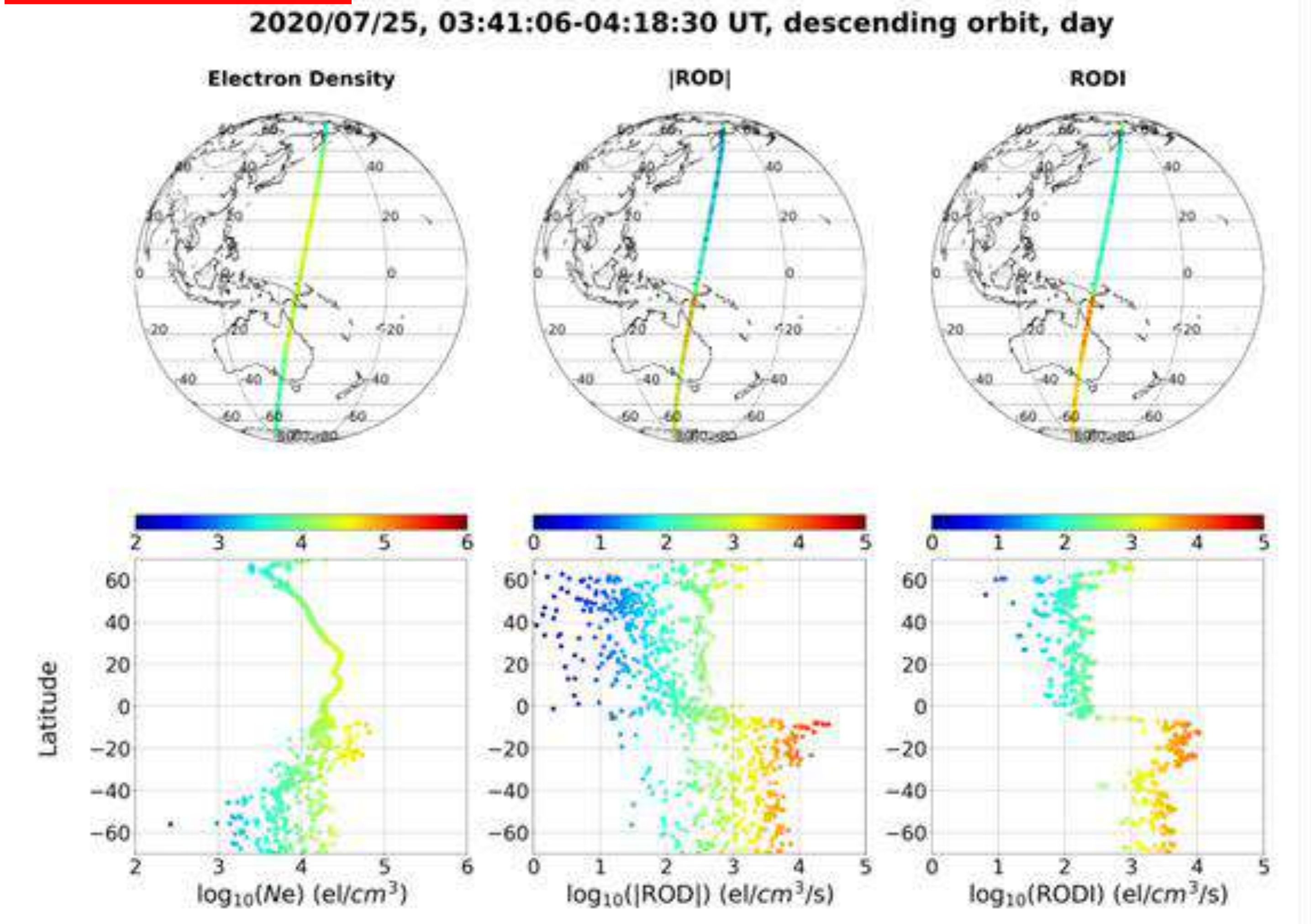

Parallel Electrical Conductivity

Giannattasio et al. (2022)

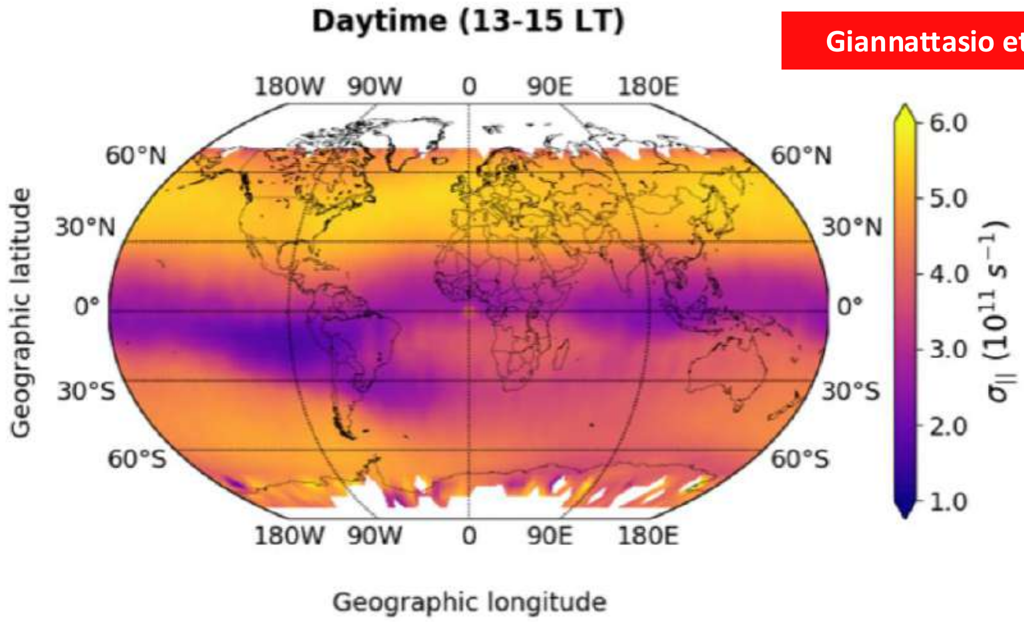

Enhanced solar ultraviolet and extreme ultraviolet radiation increases both the electron density and temperature, resulting in elevated levels of parallel conductivity.

topside ionosphere dominated by electron-ion collisions

$$\sigma_{\|} = \frac{e^2 T_e^{3/2}}{\left[34 + 4.18 \ln\left(\frac{T_e^3}{n_e}\right)\right] m_e}.$$

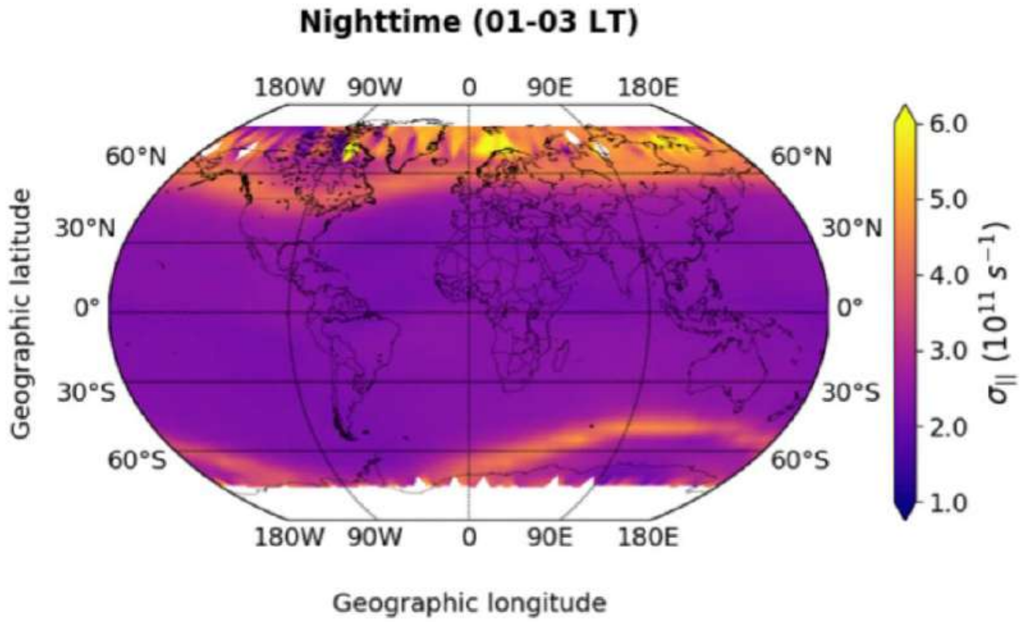

Reduction in solar input leads to a marked decrease both the electron density and temperature, except in regions located at geographic latitudes around ±60° in the nightside, where high-energy particle precipitation (mainly electrons) is known to take place.
Such particles entering the ionosphere lose little energy through collisions, their high energy translates into high electron temperature, and consequently relatively high parallel conductivity.

CSES-01

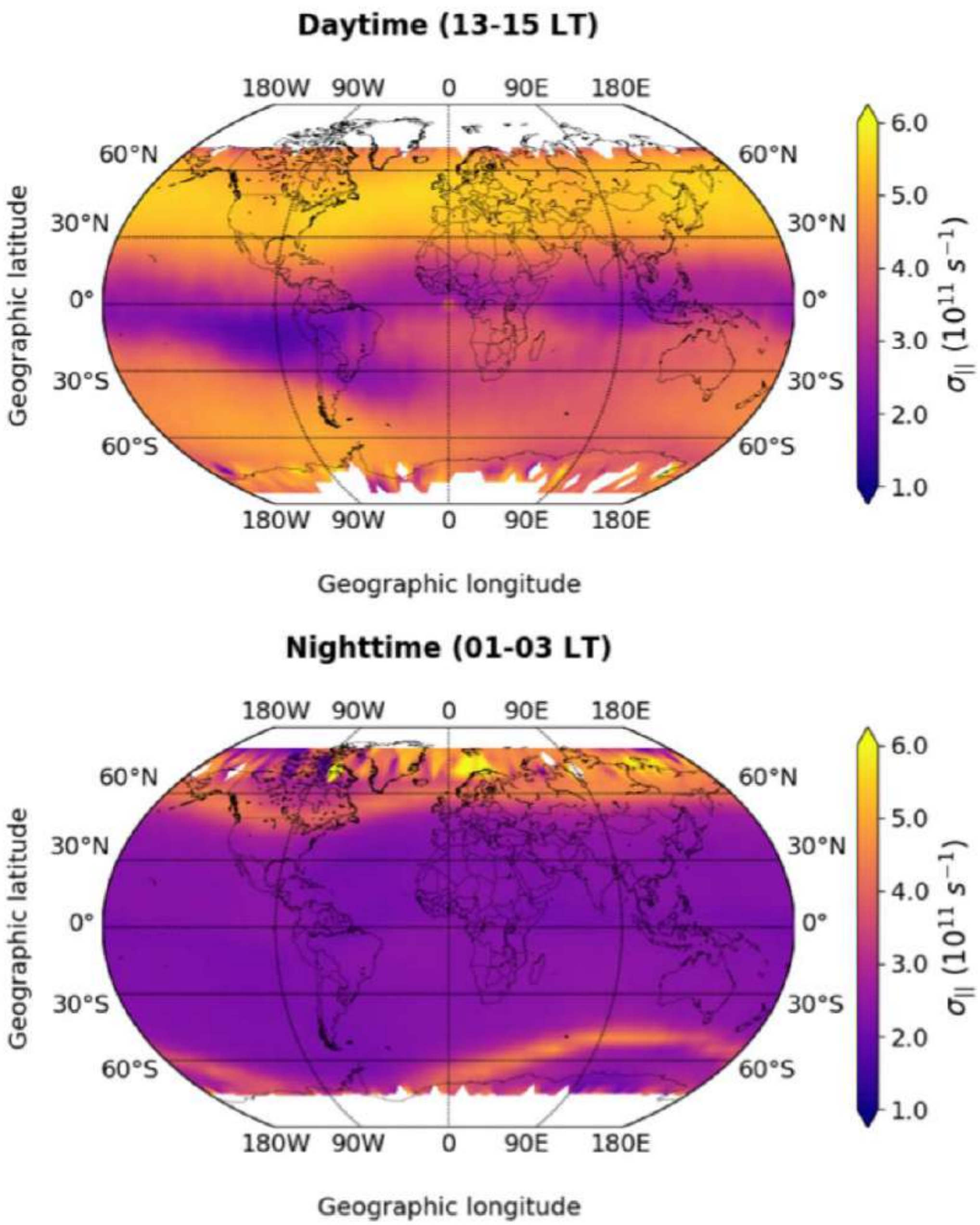

IRI model

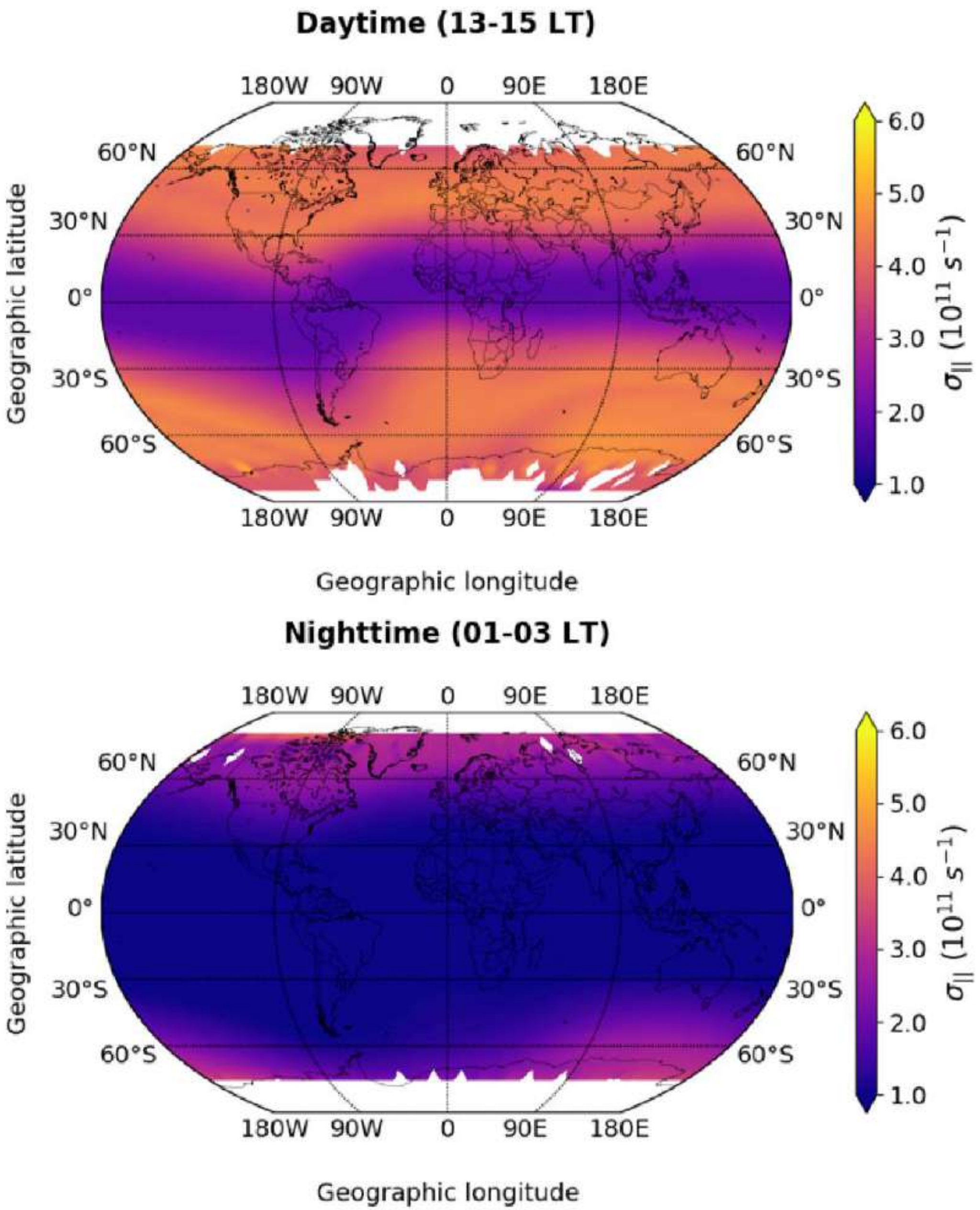

Numerical simulations of WPI in the ionosphere

Realistic ionospheric environment

IRI model

- equatorial latitudes
- morning time
- Year 2021
- 500 km of altitude

s	%	β
e	-	$1.3 \cdot 10^{-5}$
H_+	4.2	$4.2 \cdot 10^{-7}$
O_+	93.9	$9.4 \cdot 10^{-6}$

Lower plasma beta

Double species plasma

Realistic pump wave

Ambient geomagnetic field

- $\sim 10^4$nT
- Complex EM environment

Spectrum of waves

Small amplitude

First successful simulation of real ionospheric condition using a hybrid code

Plasma beta values orders of magnitude lower with respect to other works in literature

$$\frac{B}{B_0} \geq 5 \cdot 10^{-3}$$

$i.e. \sim$ hundreds of nT

Rare event (strong storm)

Real ionospheric composition at 500 km

Real plasma beta

$$\frac{B}{B_0} \leq 2 \cdot 10^{-3}$$

$i.e. \sim$ tens on nT

Not rare ionospheric disturbance

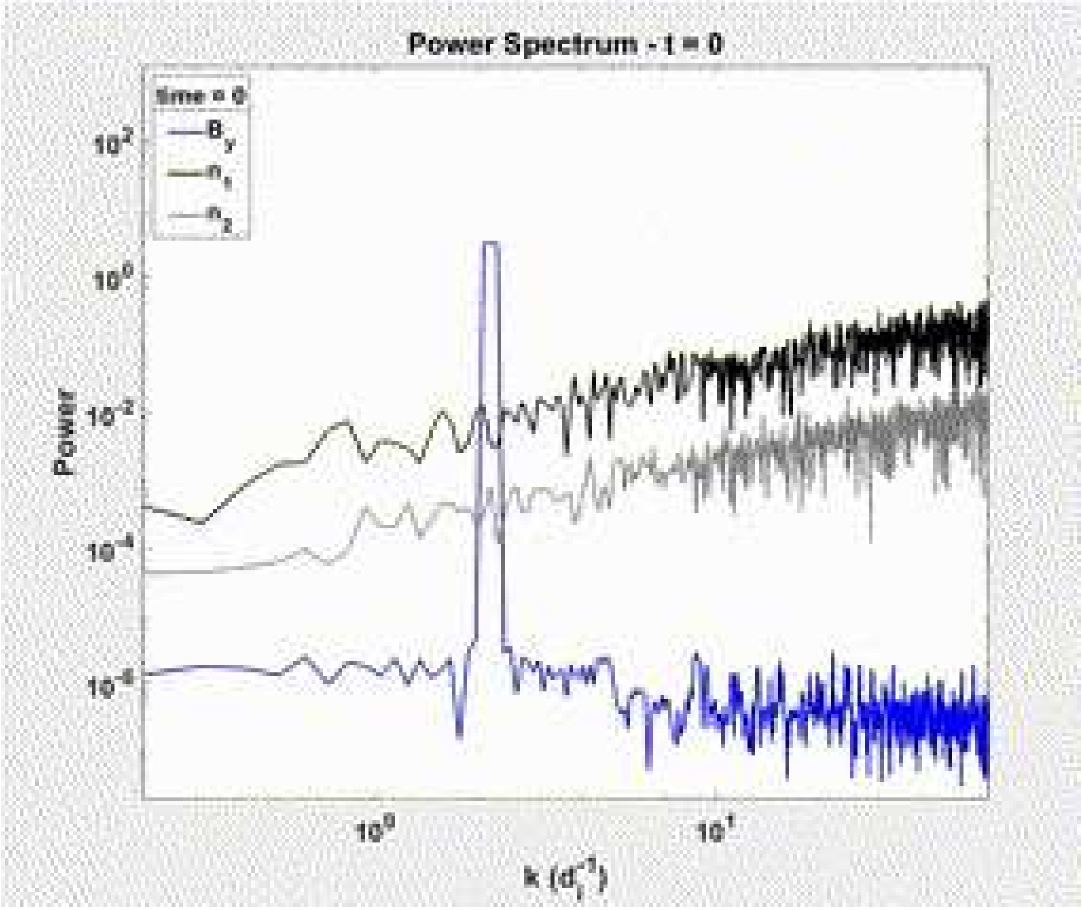

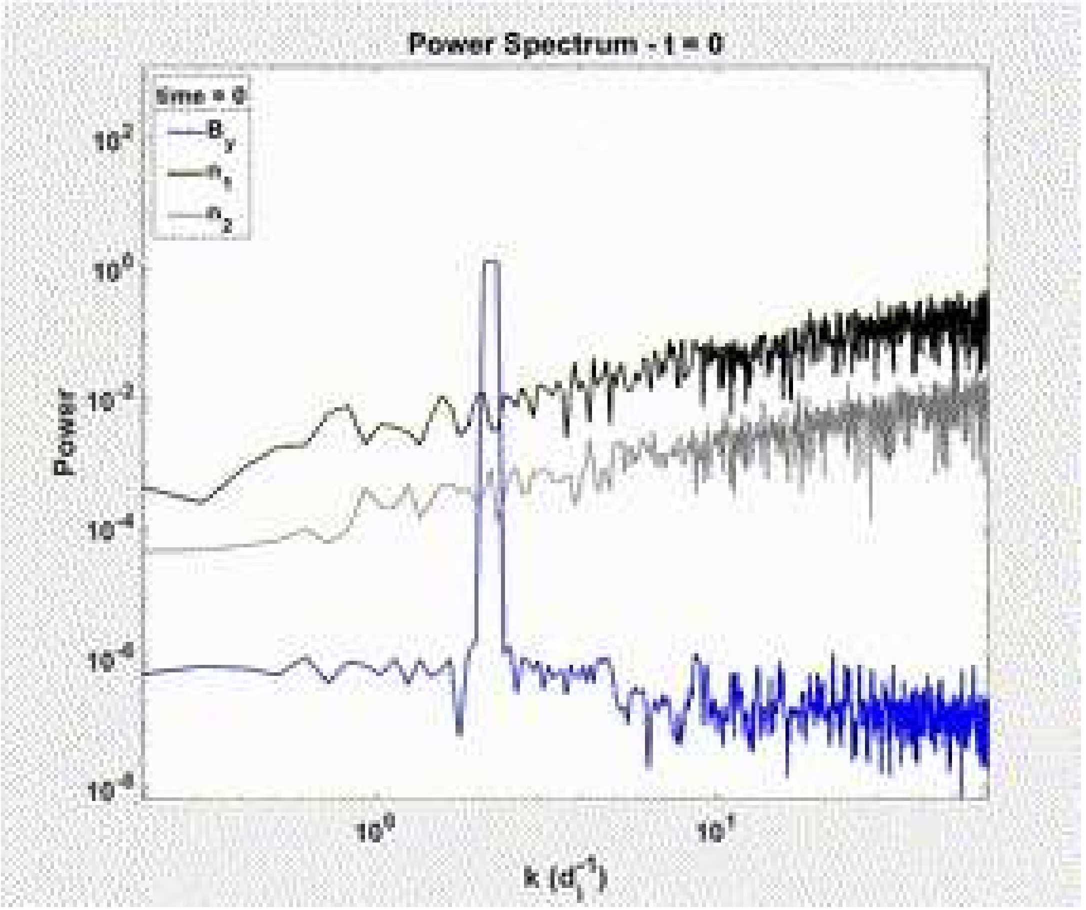

$$\frac{B}{B_0} \geq 5 \cdot 10^{-3}$$

$i.e. \sim$ hundreds of nT

Rare event (strong storm)

$$\frac{B}{B_0} \leq 2 \cdot 10^{-3}$$

$i.e. \sim$ tens on nT

Not rare ionospheric disturbance

Recchiuti et al. in prep

O^+ H^+

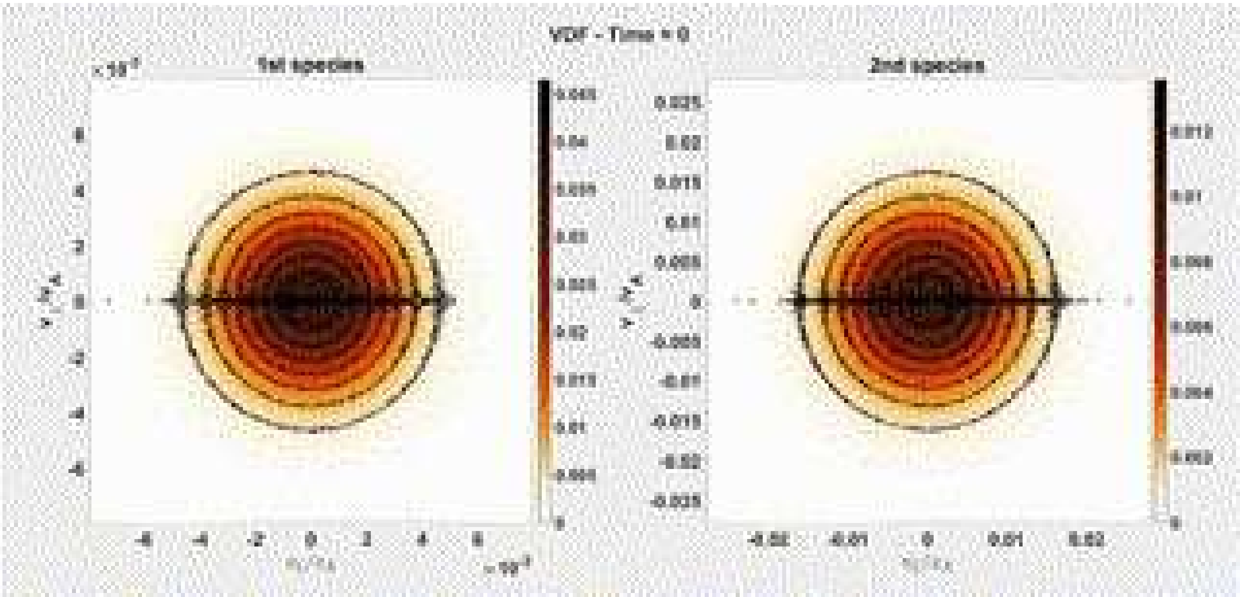

O^+ H^+

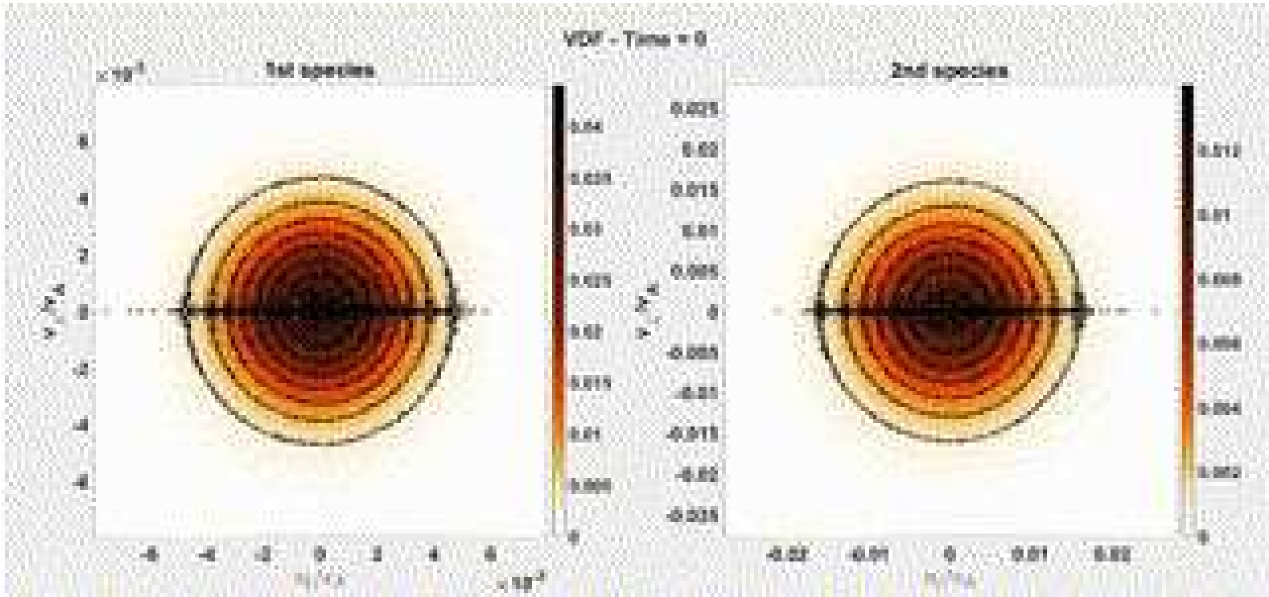

VDF rapidly broadens

Slow generation ($\sim$10 s) of fast ion beams (H_+)

Even small perturbations can induce fast ion beams in realistic conditions

Findings suggest caution when attributing concurrent event to same physical origin

Detection of ULF waves on 30 March 2021

D'Angelo et al. (2024)

CSES-01 magnetic field dynamic spectra

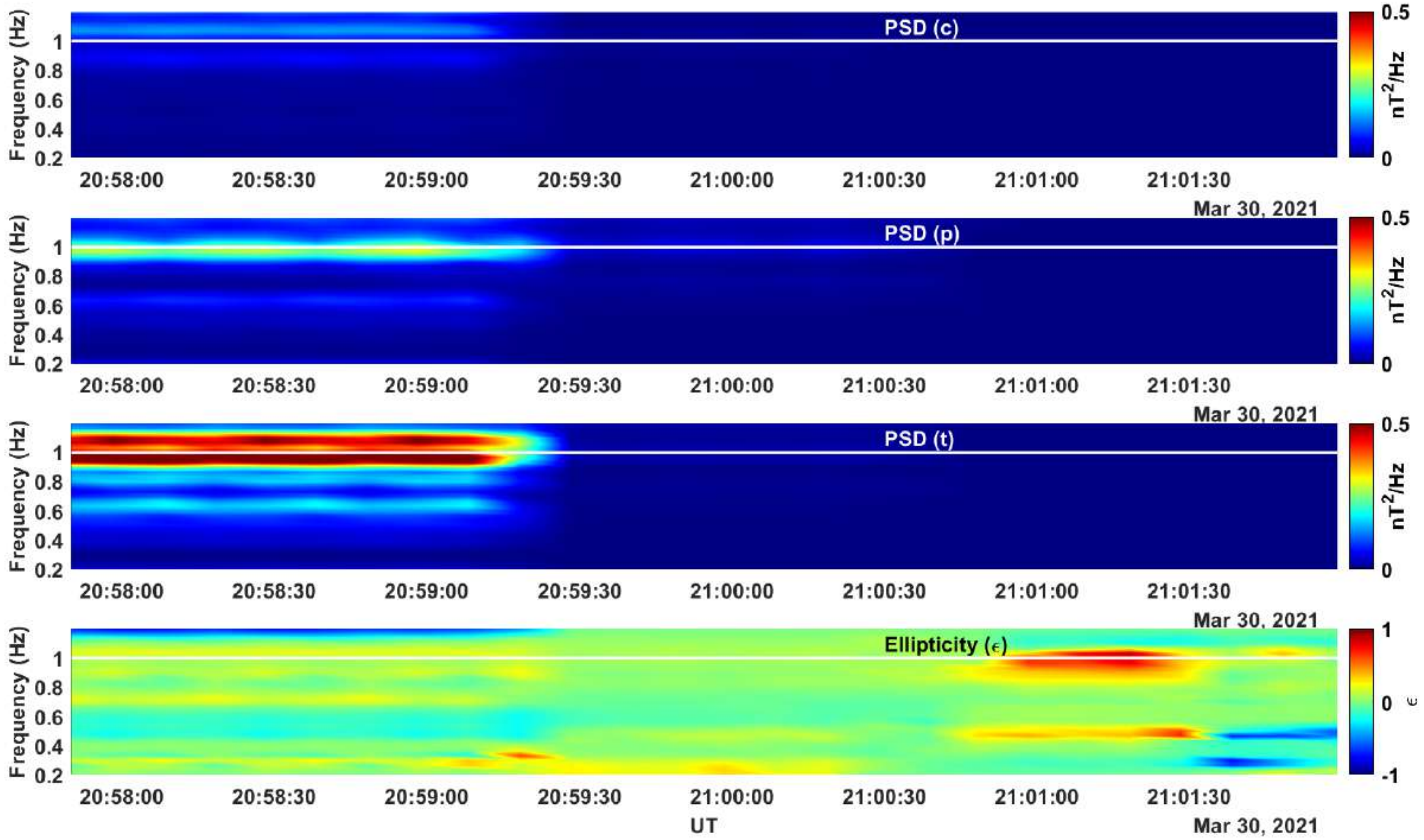

Pc1 activity between 20:58 UT and 20:59 UT in the poloidal and toroidal components, with a peculiar frequency of 1 Hz and an almost linear polarization (ε < 0.2).

Negligible activity is observed in the compressional component

MEAN FIELD ALIGNED COORDINATE SYSTEM (MFA)

COMPRESSIONAL $\hat{e_c}$ pointing the direction of the mean magnetic field;

TOROIDAL $\hat{e_t}$ pointing azimuthally as a cross product between the satellite's ran direction and the mean magnetic field;

POLOIDAL $\widehat{e_p}$ completes the triad.

Detection of ULF waves on 30 March 2021

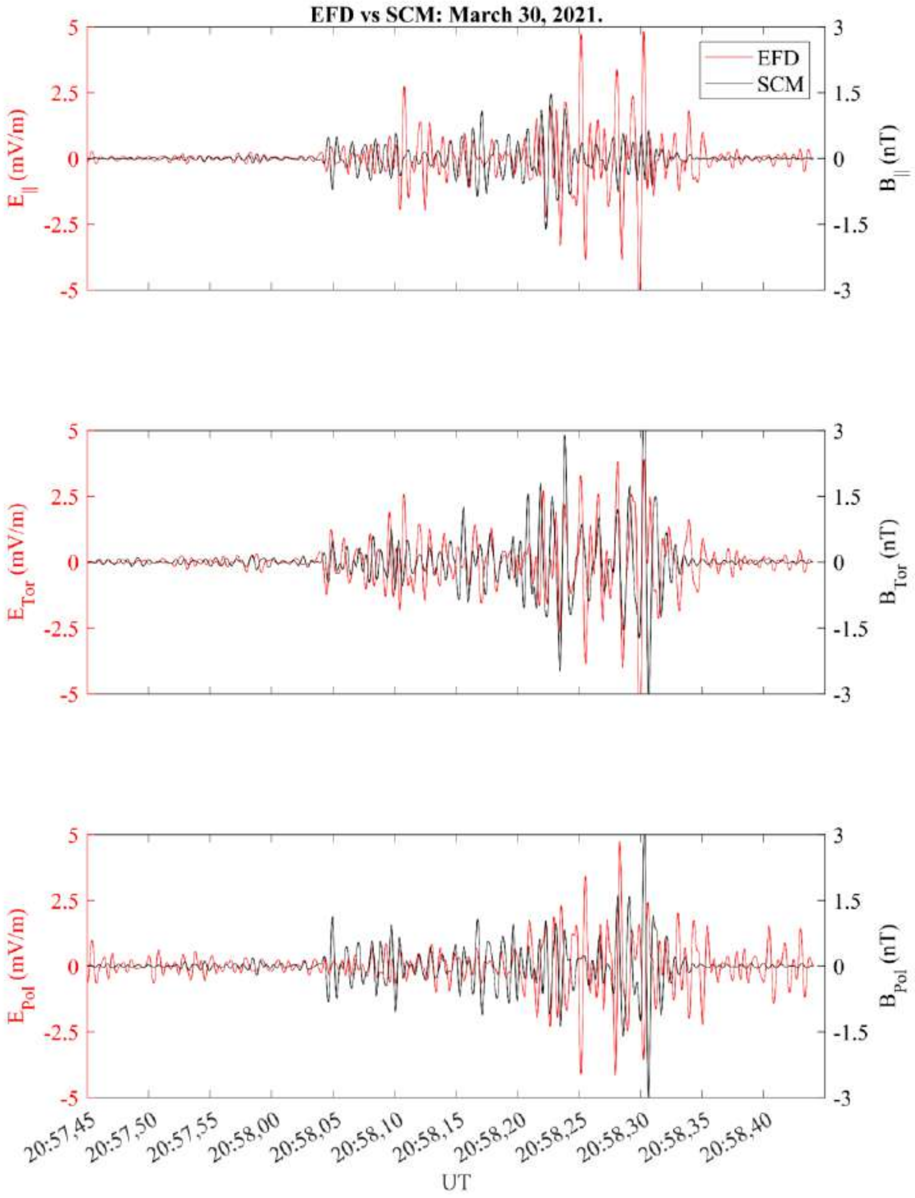

SCM AND EFD WAVEFORMS FILTERED AT 1 HZ

<u>Magnetic field fluctuations</u>: larger in components perpendicular to the local geomagnetic field

TYPICAL MARK OF TRANSVERSE ALFVÈN WAVES

<u>Electric field higher fluctuations</u>: in $E_{\parallel}$ component

CHANCE FOR PARTICLE ACCELERATION ALONG THE FIELD LINE, POSSIBLY LEADING TO PRECIPITATION

Evidences of Isolated Proton Aurora induced by ULF activity

Proton precipitation between 20:56 UT and 20:58 UT in perfect coincidence with maximum intensity of the Pc1 event captured by DMC in the magnetic H-component at ~1 Hz.

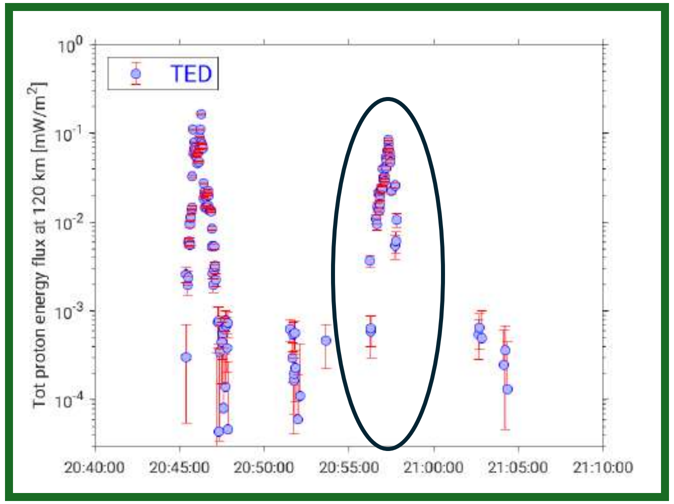

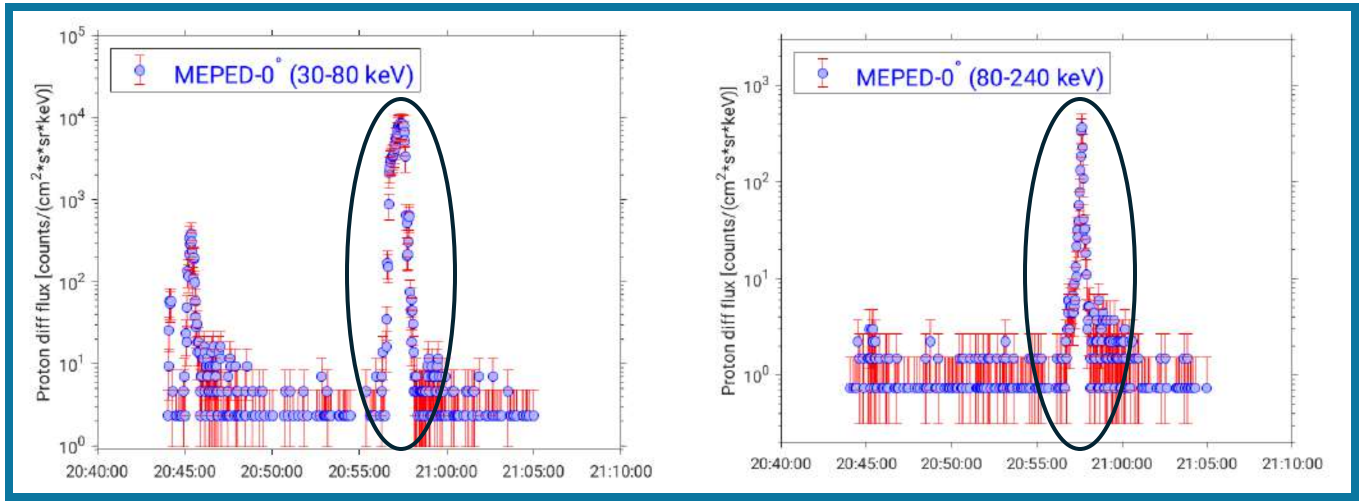

PROTONS <20 keV

RING CURRENT LIKE PROTONS

20:50 – 21:00 UT

MetOp-01 from 20:57 to 20:59 UT

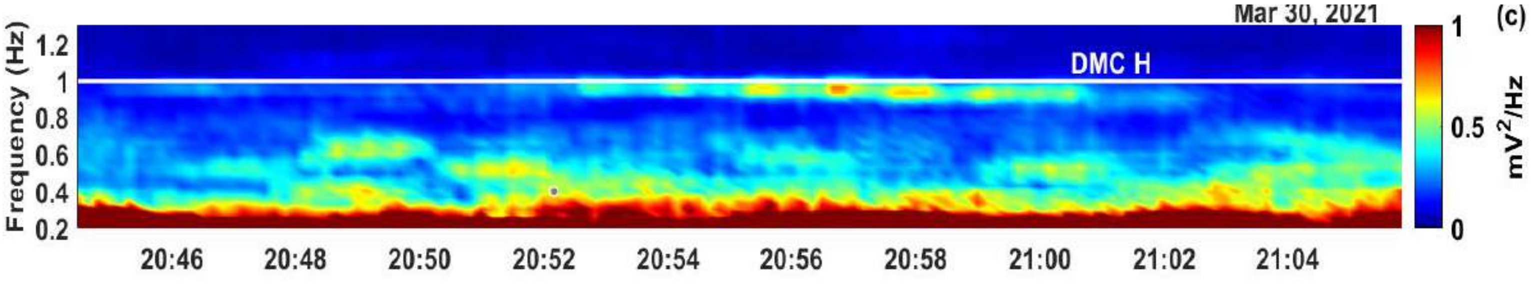

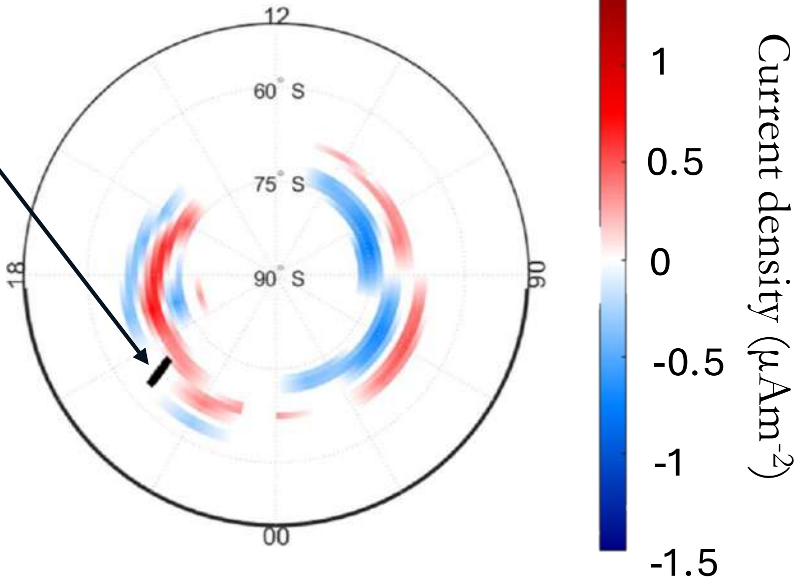

Evidences of Isolated Proton Aurora induced by ULF activity

20:57 – 20:59 UT

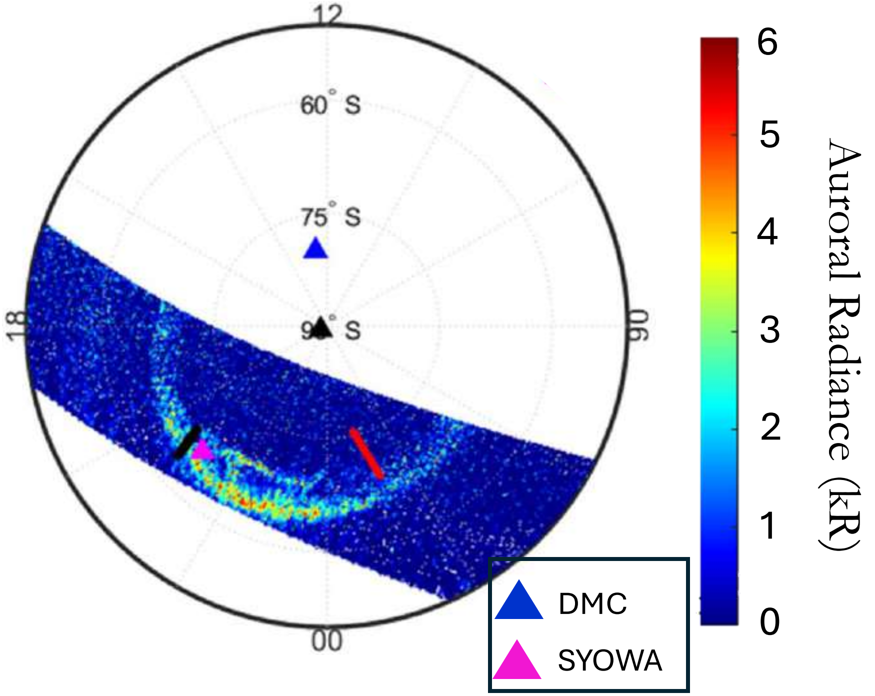

Optical keogram produced by all-sky white-light cameras located at Syowa

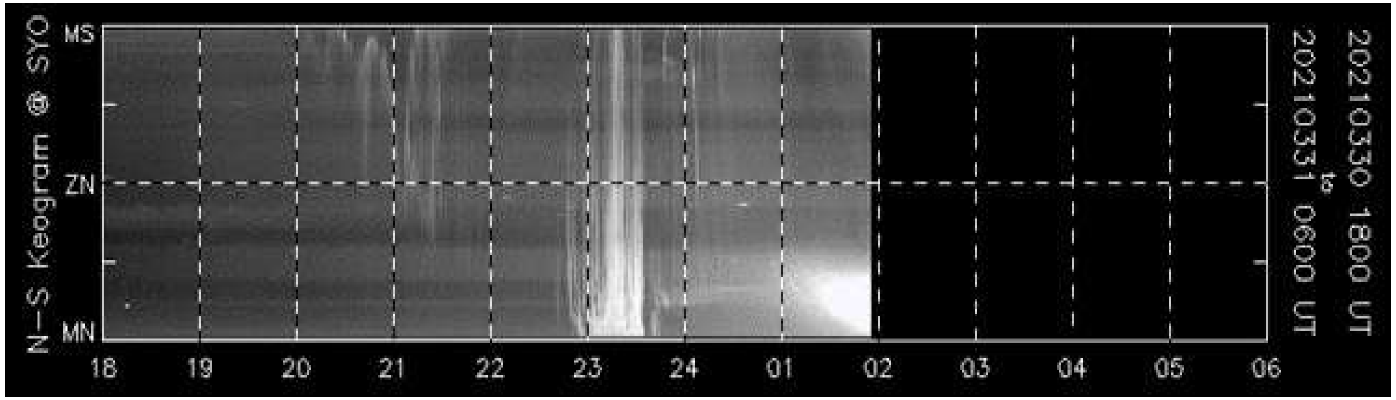

- ❖ In the same magnetic sector affected by proton precipitation HI emission has been also recorded.
- ❖ A clear isolated arc is clearly visible in the same region marked by the proton precipitation spotted by DMSP/SSUSI imagers.
- ❖ Observed ULF waves at ~1 Hz probably have their source in a magnetospheric equatorial region at L ~ 6.6/6.7 in the evening/night sector, not far from plasmapause.

Plasmaspheric model

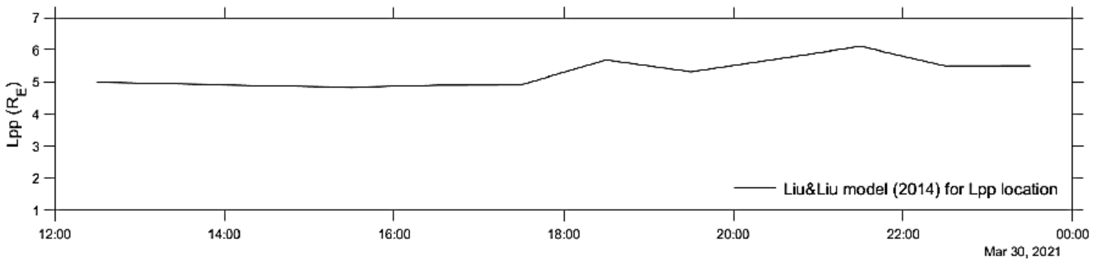

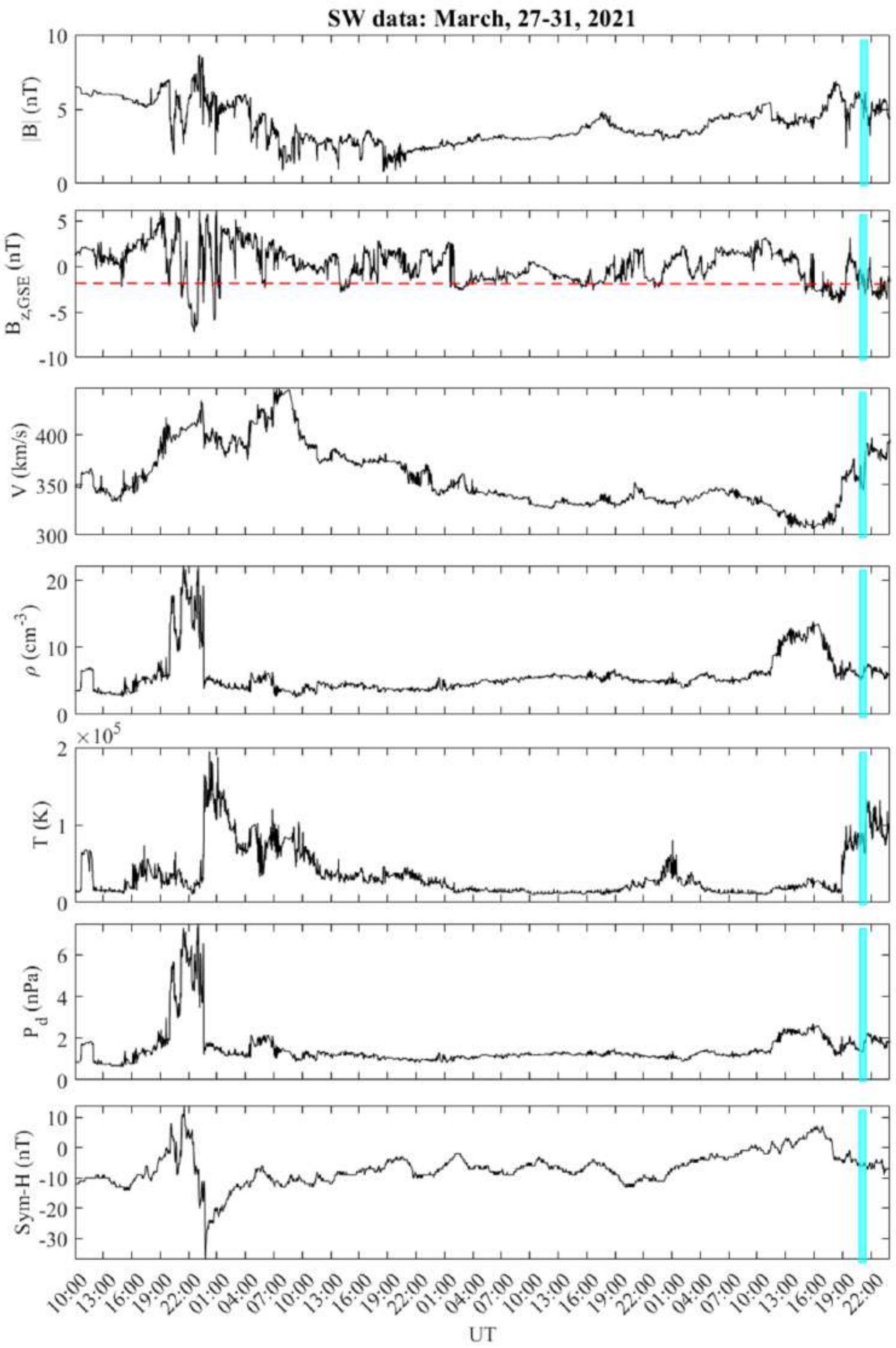

Observations of ULF waves detected on 30th March 2021

- **27 MARCH 2021:** a weak storm (SYM-H minimum value: ~-40 nT) occurred in correspondence with the southward turning of the IMF (between 21:00 UT and 23:00 UT), followed by a long recovery phase corresponding to a fluctuating $B_{z,IMF}$.

- **30 MARCH 2021:** Pc1 event (~20:44-21:06 UT)
  - at a near zero IMF,
  - upon a small increase in the solar wind dynamic pressure,
  - under low Kp,
  - low Sym-H,
  - moderate AE conditions.

Characterization of the spatiotemporal scales of the high-latitudes ionospheric electric field

Papini et al. (2023)

Identification and characterization of electric field variability at high latitudes related to FACs activity and particle precipitation.

Technique for the automatic identification of orbital intervals characterized by such intense activity

FIRST DATABASE OF EVENTS

Two distinct plasma environments:

- FAC activity in the AO;
- Polar Cap activity;

Two distinct activity level:

- Disturbed (top panel);
- Quiet (bottom panel);

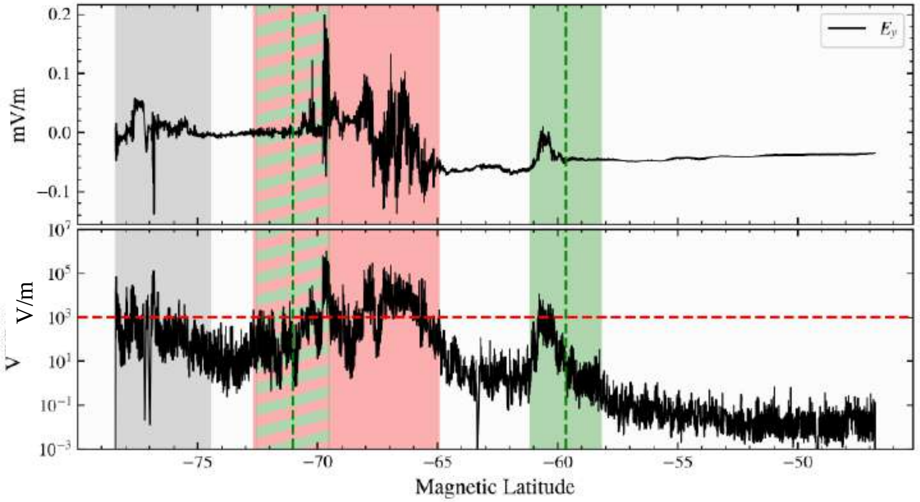

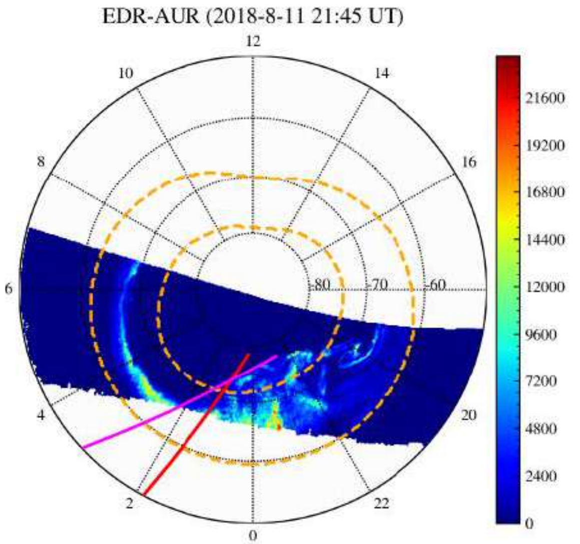

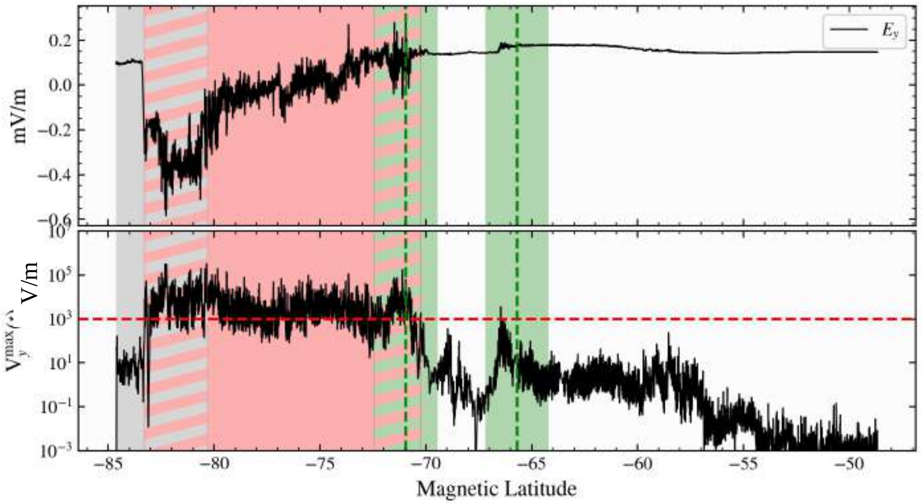

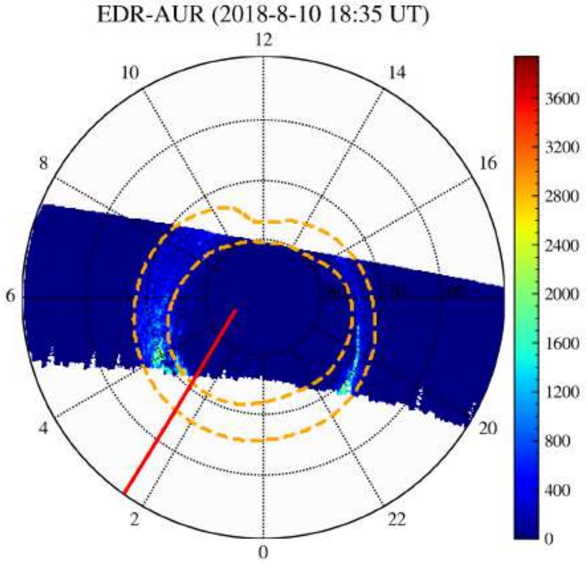

Statistical analysis of the power distribution

Papini et al. in prep.

<u>Histogram of electric power as a function of:</u>

- latitudinal extension of the interval (left column);
- magnetic latitude of the interval (right column);

1. A clear dependence of the power with magnetic latitude is present.
2. Concentration of the latitudinal extension about two degrees (corresponding to ~200 km), likely due to the size of the active electromagnetic structures (e.g. FACs).

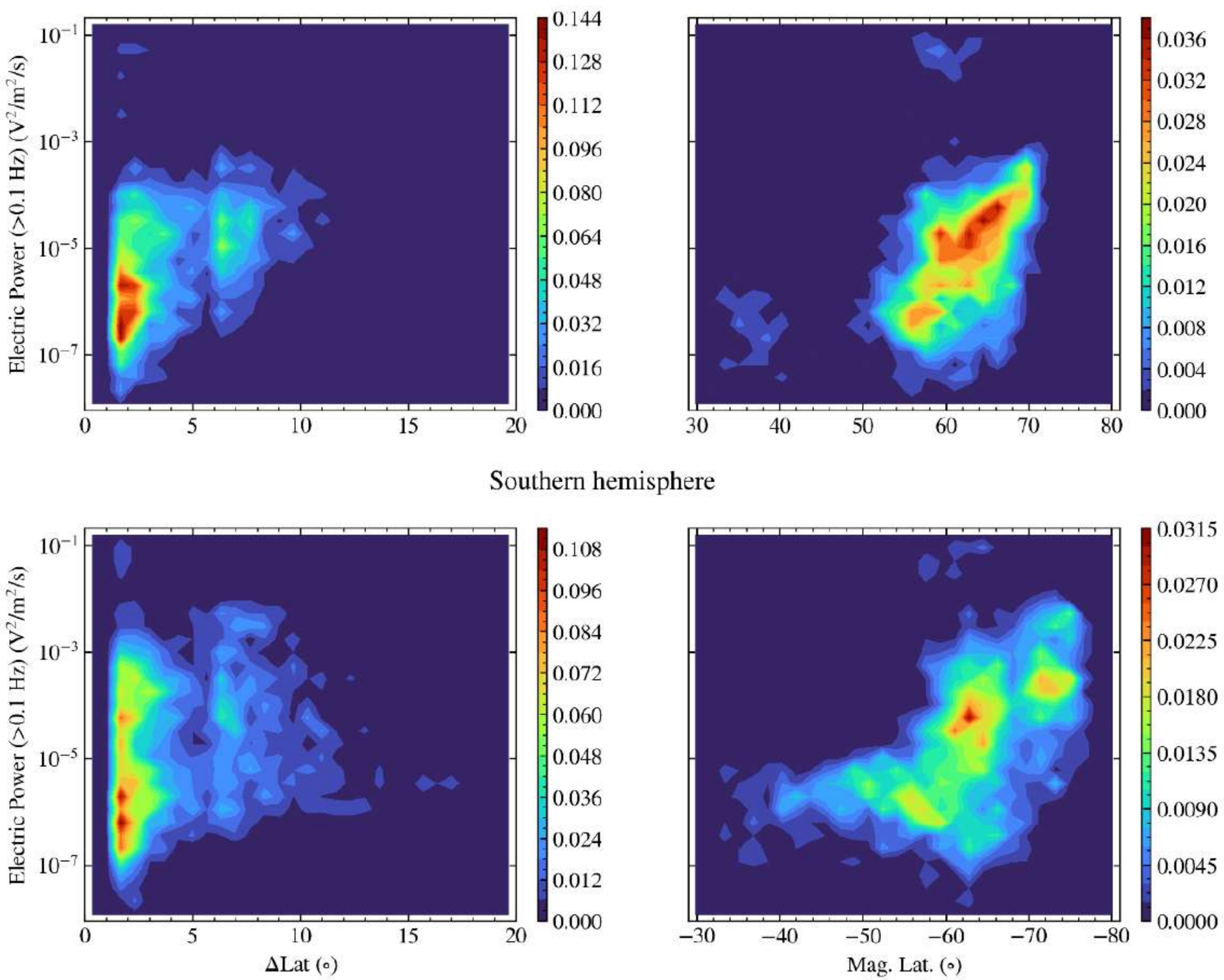

background for anomaly detection

Characterization of of the background electric field due to ionospheric convection

Study of the ionospheric **E x B velocity** drift at high latitudes.

$$\overrightarrow{v_D} = \frac{\vec{E} \times \vec{B}}{B^2}$$

The multifractal analysis revealed the occurrence of 2D convective turbulence from tens of kilometers (typical size of FACs) down to tens of meters (electronic dissipative scales), thanks to the unmatched resolution of EFD-01. Such dynamics is characterized by the presence of filamentary thin tube-like structuring (possibly connected to FACs variability).

fluctuations of the drift velocity

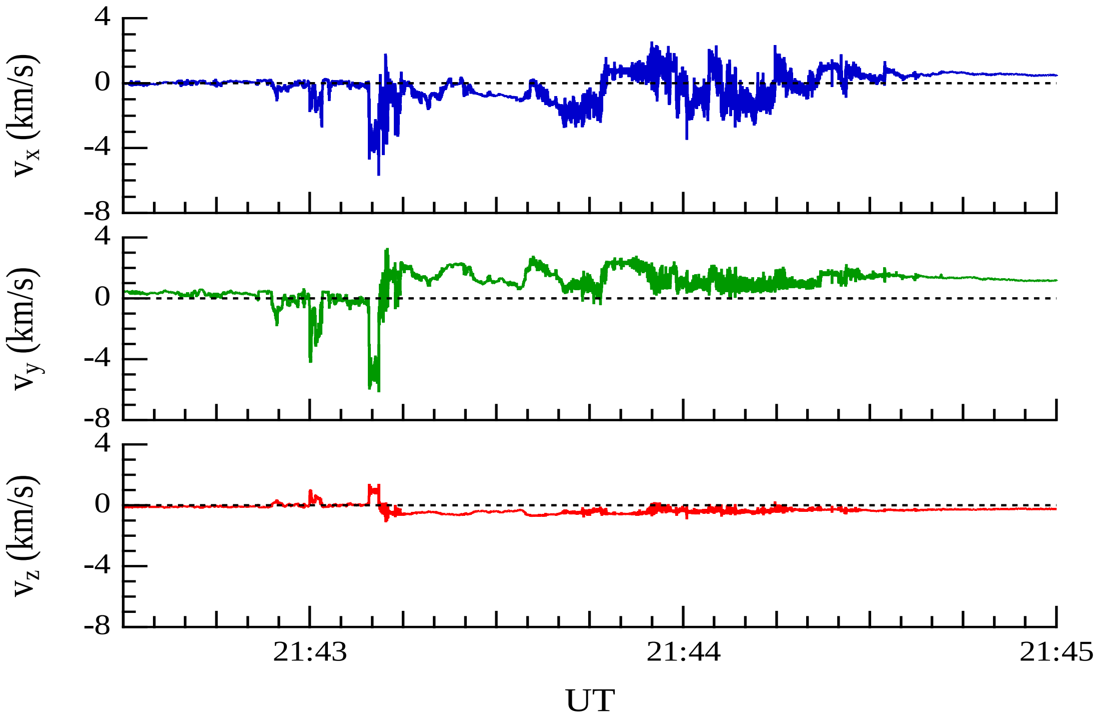

scaling exponents associated with fluctuations

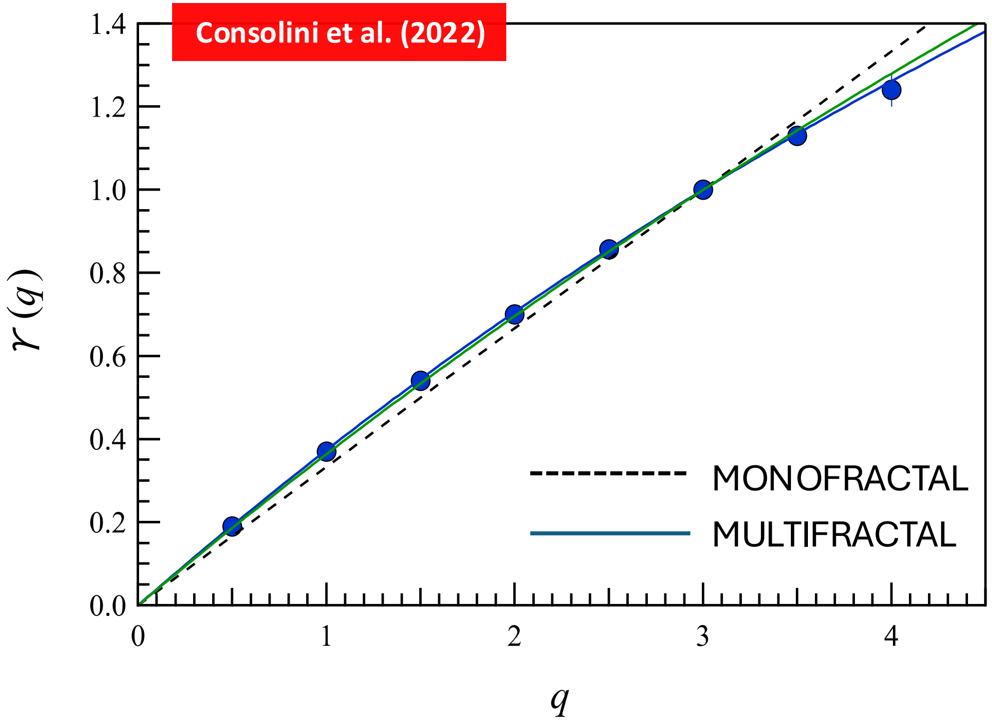

These measurements also allow us to advance our knowledge of the ionospheric dissipative structure

Stochastic nature of the polar ionospheric fluctuations

Further step in the characterization of the electric field fluctuations in the polar ionosphere to gain knowledge on the nature of particle precipitation at those latitudes.

Data-driven numerical modelling of high latitude electric field fluctuations in which fluctuations can be numerically modeled using the Langevin Equation, which allow to numerically simulate (and thus reproduce) their properties.

- electric field fluctuations in the range 2.5 Hz ≤ f ≤ 25 Hz, i.e., from 3 km down to few hundred meters, behave stochastically, with a Markovian character.
- At higher frequencies, such behavior disappear, due to either kinetic processes and/or energy dissipation.

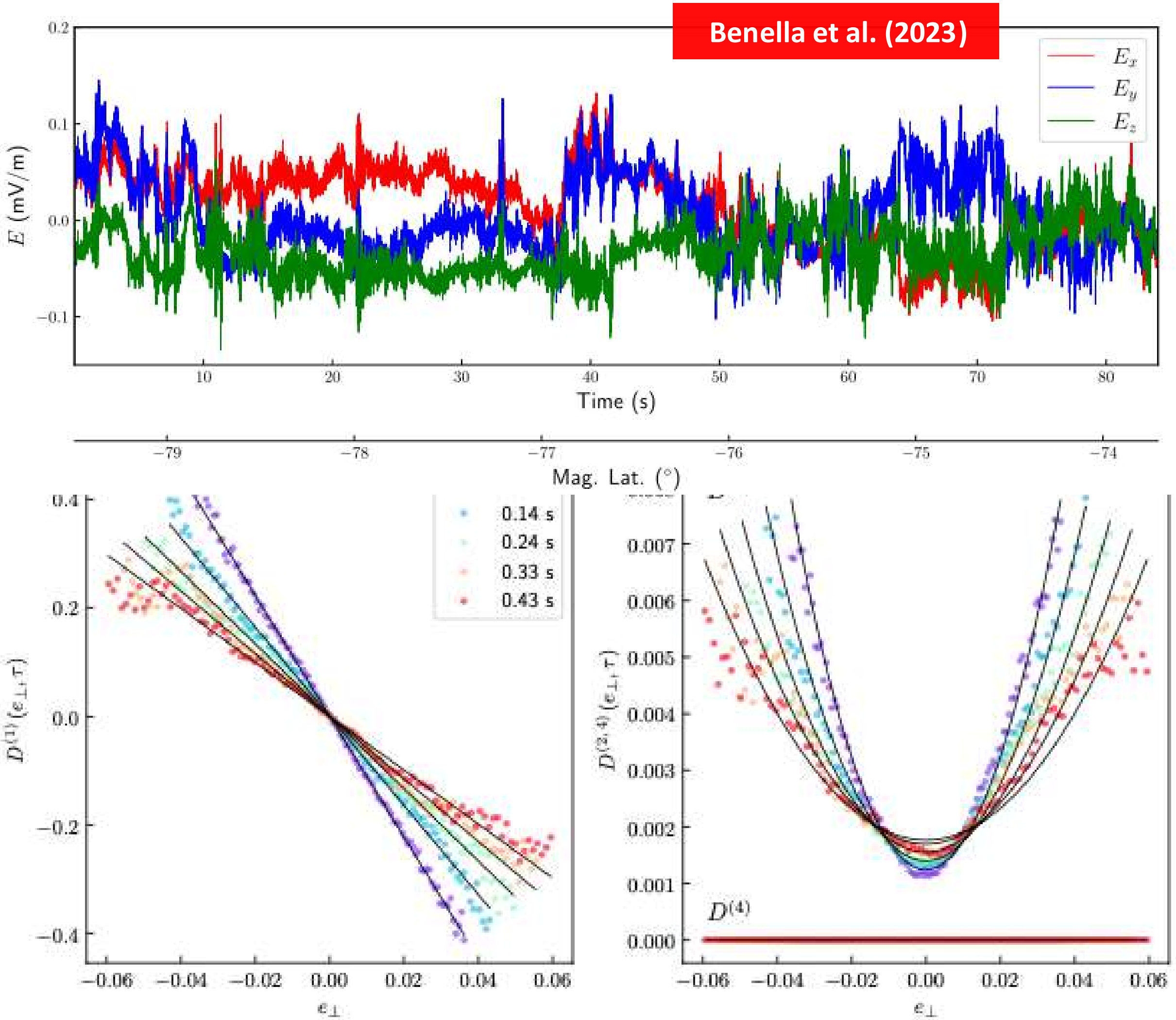

capability of numerically reproduce/predict the behaviour of electric fluctuations potentially provide a diagnostics for the detection of anomalous behaviour/signals of an origin different than the usual ionospheric dynamics

LAP & EFD Calibrations

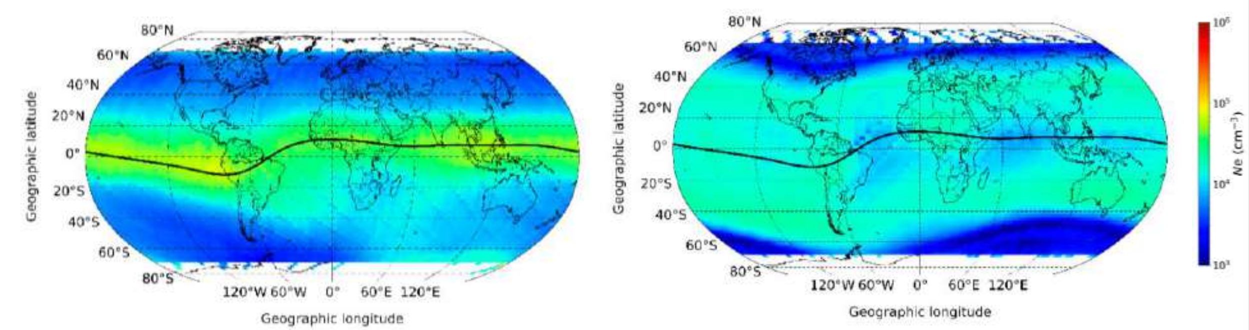

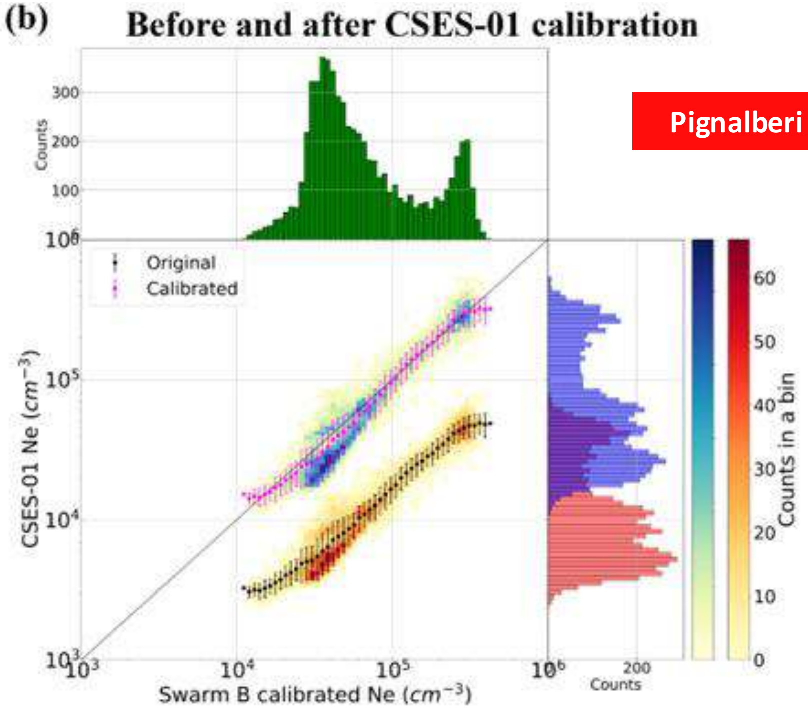

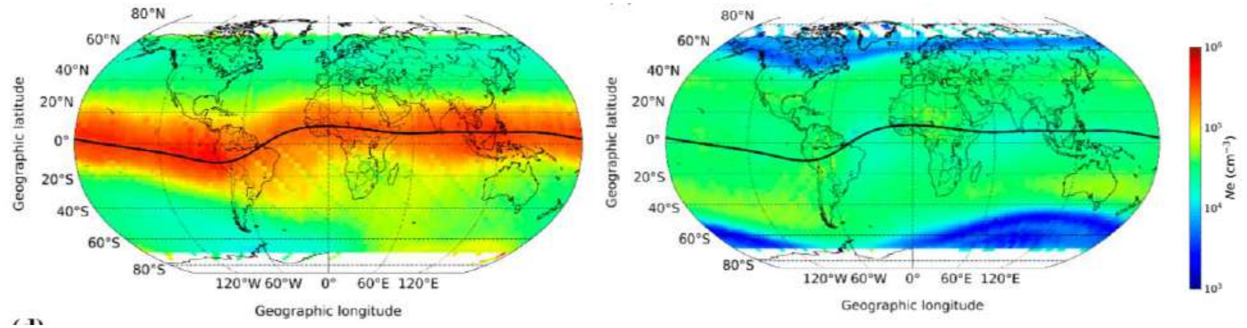

Pignalberi et (2022)

```
EFD-01 L2 -> L2Limadou data processor (Limadou Scienza+ project)

usage: ./efd01_reprocesstoL2Limadou.py <options>

EFD-01 L2 -> L2Limadou data processor
```

Program for calibration/correction of EFD-01 L2 Files

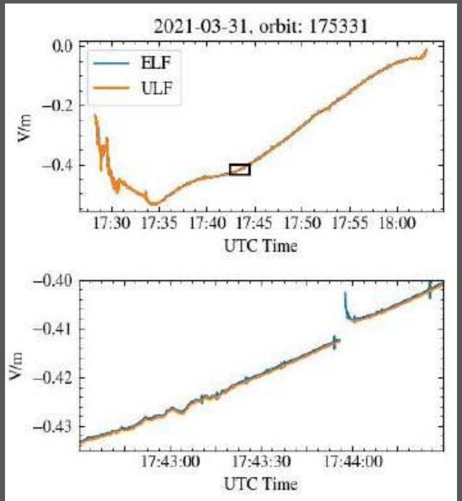

1. Presence of gaps in the data: data are filled with desired value, and gaps are labelled.
2. Spikes after gaps are identified and labeled.

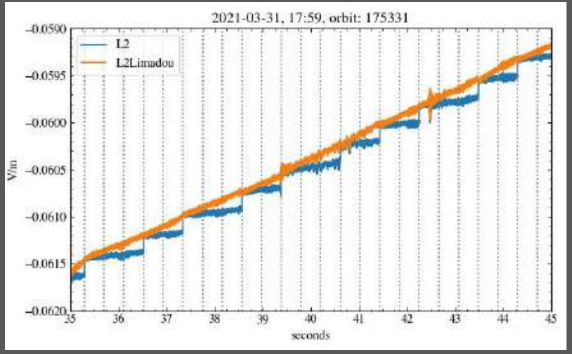

3. Correcting for systematic jumps in the waveforms introduced by errors in rotating the electric field components to the WGS84 Cartesian frame (Rotational drift):

$$\vec{E}_{i,\mathrm{derot}} = \mathrm{SLERP}(t_i; \mathrm{I}, \mathrm{R}, 0, 1) \cdot \vec{E}_i$$

Papini et al. in prep.

Publications in the frame of Scienza + (1/3)

1. Benella et al. (2023) Modeling turbulent fluctuations in high-latitude ionospheric plasma using electric field CSES-01 observations. Atmosphere, 14, 1466.
2. Carbone et al. (2023) Nonlinear shallow water investigation of atmospheric disturbances generated by strong seismic events. Physical Review E.
3. Cicone et al. (2021) Auroral oval layers detection by using CSES plasma and electric field data. Nuovo Cimento, 44C, 117.
4. Consolini et al. (2021) Electric Field Multifractal Features in the High-Latitude Ionosphere: CSES-01 Observations, Atmosphere, 12, 646.
5. Consolini et al. (2022) On Turbulent Featuresof ExB Plasma Motion in the Auroral Topside Ionosphere: Some Results from CSES-01 Satellite. Remote Sensing 14, 1936.
6. D’Angelo et al. (2021) Investigation of the physical processes involved in the GNSS amplitude scintillations at high-latitude: a case study, Remote Sensing, 13, 2493.
7. D’Angelo et al. (2021) Analysis of the August 14, 2018 plasma bubble by CSES satellite, Il Nuovo Cimento C.
8. D’Angelo et al. (2022) Haiti Earthquake (Mw 7.2): Magnetospheric-Ionospheric-Lithospheric Coupling during and after the Main Shock on 14 August 2021, Remote Sensing, vol. 14, p. 5340.
9. D’Angelo et al. (2025) Detecting Post-midnight plasma depletions through plasma density and electric field measurements in the low-latitude ionosphere. Under revision on Remote Sensing.
10. D’Angelo et al. (2024). A Case Study of Pc1 Waves Observed at the Polar Cap Associated with Proton Precipitation at Subauroral Latitudes. Atmosphere, 15(2), 219.
11. De Michelis et al. (2025). A Dynamical System Analysis of Electric Field Fluctuations inside Equatorial Plasma Bubbles: A Case study Using CSES-01 Observations. Under revision on Geophysical Research Letters
12. De Micheliset al. (2024) Investigating Equatorial Plasma Depletions through CSES-01 Satellite Data. Atmosphere 15, 868.

Publications in the frame of Scienza + (2/3)

13. De Santis et al (2023) Near-Earth electromagnetic environment and natural hazard disturbances: Volume I, Front. Environ. Sci.
14. Giannattasio et al. (2022) Parallel Electrical Conductivity at Low and Middle Latitudes in the Topside Ionosphere Derived from CSES-01 Measurements. Remote Sensing, 14, 5079.
15. Hu et al. (2022) A large-scale magnetospheric line radiation event in the upper ionosphere recorded by China-Seismo-Electromagnetic Satellite, Journal of Geophysical Research: Space Physics, Volume 128, Issue 2.
16. Oliveira et al. (2024) Predicting Interplanetary Shock Occurrence for Solar Cycle 25: Opportunities and Challenges in Space Weather Research, Space Weather, 22.
17. Papini et al. (2023) Detecting the auroral oval through CSES-01 electric field measurements in the ionosphere. Remote Sensing 2023, 15, 1568.
18. Pezzopane et al. (2022) On the best settings to calculate ionospheric irregularity indices from in-situ plasma parameters of CSES-01. IEEE JSTARS 2022, 15, 4058.
19. Piersanti et al. (2021) On the Geomagnetic Field Line Resonance Eigenfrequency Variations during Seismic Event. Remote Sensing; 13(14):2839
20. Piersanti et al. (2022) On the source of the anomalous June 23, 2020 ULF waves detected at both ground and satellite data, J. Geophys. Res.
21. Piersanti et al. (2022) On the magnetosphere-ionosphere coupling during the May 2021 Geomagnetic storm, Space Weather 20(6).
22. Piersanti et al. (2025) Multiscale analysis of the background seismicity: application to Campi Flegrei (Italy), JGR-Solid Earth, in press.
23. Piersanti et al. (2023) Evidence of an upper ionospheric electric field perturbation correlated with gamma ray burst, Nature Communication.
24. Piersanti et al. (2025) On the Ionosphere–Atmosphere–Lithosphere Coupling During the 9 November 2022 Italian Earthquake. Geosciences , 15, 22.

Publications in the frame of Scienza + (3/3)

25. Piersanti et al. (2025). On the geoelectric field response to the SSC of the May 2024 super storm over Europe, Space Weather, 23.
26. Pignalberi et al (2023) Modelling the topside ionosphere effective scale height through in-situ electron density observations by low-Earth-orbit satellites, Universe, 9, 280.
27. Pignalberi et al. (2022) Inter-calibration and statistical validation of topside ionosphere electron density observations made by CSES-01 mission. Remote Sensing, 14, 4079.
28. Quattrociocchi et al. (2024) Characterization of Electric Field Fluctuations in the High-Latitude Ionosphere Using a Dynamical Systems Approach: CSES-01 Observations. Remote Sensing, 16, 3919.
29. Rebustini et al. (2022) Calibration of the Electric Field Detector for the CSES-02 satellite, Il Nuovo Cimento C.
30. Recchiuti et al. (2023) Detection of electromagnetic anomalies over seismic regions during two strong (MW > 5) earthquakes. Frontiers in Earth Science, vol. 11.
31. Xiong et al., (2022) Solar flux influence on the in-situ plasma density at topside ionosphere measured by Swarm and CSES01 satellites, J. Geophys. Res.
32. Zhima et al. (2021), Storm-time features of the ionospheric ELF/VLF waves and energetic electron fluxes revealed by the China Seismo-Electromagnetic Satellite, Appl. Sci. 11(6), 2617.


Eurasion plate
North American plate
African plate
Indo-Australian plate
Nazca plate
Antarctic plate
Thank you!